[American Journal of Science, Vol. 310, November, 2010, P. 981–1023, DOI 10.2475/09.2010.09]

THE RIO APA CRATON IN MATO GROSSO DO SUL (BRAZIL) AND NORTHERN PARAGUAY: GEOCHRONOLOGICAL EVOLUTION, CORRELATIONS AND TECTONIC IMPLICATIONS FOR RODINIA AND GONDWANA

UMBERTO G. CORDANI*,†, WILSON TEIXEIRA*, COLOMBO C. G. TASSINARI*, JOSÉ M. V. COUTINHO*, and AMARILDO S. RUIZ**

ABSTRACT. The Rio Apa cratonic fragment crops out in Mato Grosso do Sul State of Brazil and in northeastern Paraguay. It comprises Paleo-Mesoproterozoic medium grade metamorphic rocks, intruded by granitic rocks, and is covered by the Neoproterozoic deposits of the Corumbá and Itapocumi Groups. Eastward it is bound by the southern portion of the Paraguay belt. In this work, more than 100 isotopic determinations, including U-Pb SHRIMP zircon ages, Rb-Sr and Sm-Nd whole-rock determinations, as well as K-Ar and Ar-Ar mineral ages, were reassessed in order to obtain a complete picture of its regional geological history.

The tectonic evolution of the Rio Apa Craton starts with the formation of a series of magmatic arc complexes. The oldest U-Pb SHRIMP zircon age comes from a banded gneiss collected in the northern part of the region, with an age of 1950 ± 23 Ma. The large granitic intrusion of the Alumiador Batholith yielded a U-Pb zircon age of 1839 ± 33 Ma, and from the southeastern part of the area two orthogneisses gave zircon U-Pb ages of 1774 ± 26 Ma and 1721 ± 25 Ma. These may be coeval with the Alto Tererê metamorphic rocks of the northeastern corner, intruded in their turn by the Baía das Garças granitic rocks, one of them yielding a zircon U-Pb age of 1754 ± 49 Ma. The original magmatic protoliths of these rocks involved some crustal component, as indicated by the Sm-Nd T_{DM} model ages, between 1.9 and 2.5 Ga. Regional Sr isotopic homogenization, associated with tectonic deformation and medium-grade metamorphism occurred at approximately 1670 Ma, as suggested by Rb-Sr whole rock reference isochrons. Finally, at 1300 Ma ago, the Ar work indicates that the Rio Apa Craton was affected by widespread regional heating, when the temperature probably exceeded 350°C.

Geographic distribution, age and isotopic signature of the lithotectonic units suggest the existence of a major suture separating two different tectonic domains, juxtaposed at about 1670 Ma. From that time on, the unified Rio Apa continental block behaved as one coherent and stable tectonic unit. It correlates well with the SW corner of the Amazonian Craton, where the medium-grade rocks of the Juruena-Rio Negro tectonic province, with ages between 1600 and 1780 Ma, were reworked at about 1300 Ma. Looking at the largest scale, the Rio Apa Craton is probably attached to the larger Amazonian Craton, and the actual configuration of southwestern South America is possibly due to a complex arrangement of allochthonous blocks such as the Arequipa, Antofalla and Pampia, with different sizes, that may have originated as disrupted parts of either Laurentia or Amazonia, and were trapped during later collisions of these continental masses.

Key words: Rio Apa Craton, Geochronology, South America, Tectonic evolution, Geotectonic correlations.

INTRODUCTION

The Rio Apa cratonic fragment, which is located in the central part of South America (fig. 1) and measures 220 km long × 60 km wide, is poorly exposed, being

* Institute of Geosciences, University of São Paulo, Rua do Lago 562, 05508-080, São Paulo, SP, Brazil
** Institute of Geosciences, Federal University of Mato Grosso, Av Fernando Correia s/n, 09923-900 Cuiabá, MT, Brazil
† Corresponding author: ucordani@usp.br

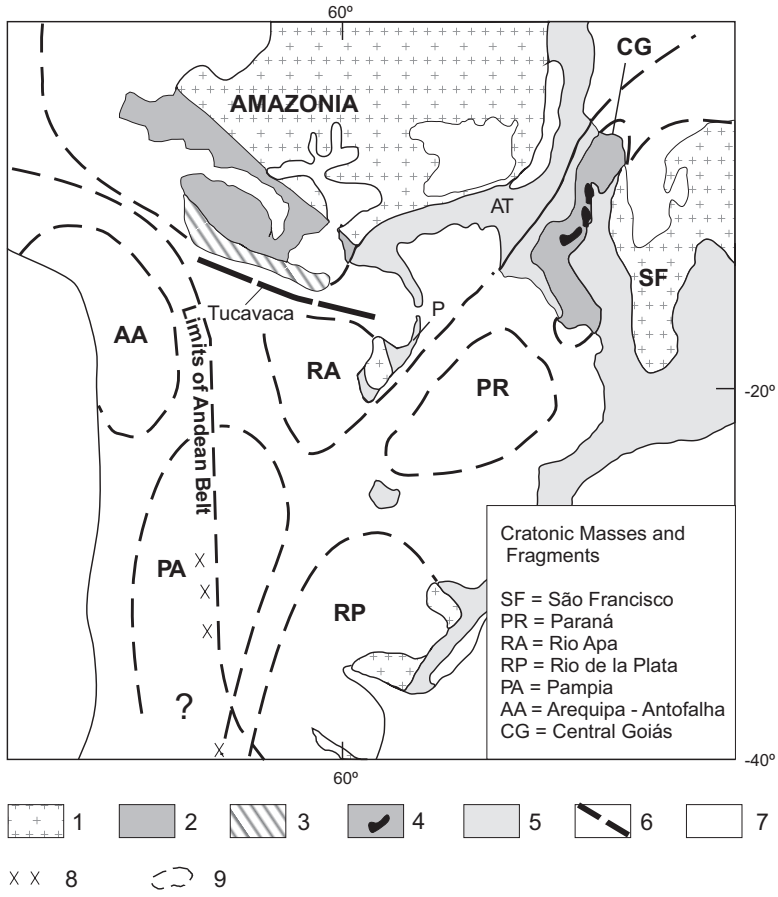

Fig. 1. Geotectonic sketch of Central South America, showing the Rio Apa Craton as an allochthonous tectonic feature, attached to the Amazonian Craton in the process of agglutination of Gondwana (adapted from Kröner and Cordani (2003). 1—Cratonic areas, including the Rondonian-San Ignácio (2) and Sunsás (3) belts (in Amazonia); 4—Central Goiás Massif, including large mafic complexes; 5—Neoproterozoic tectonic provinces (for example, P—Paraguay and AT—Araguaia-Tocantins belts); 6—Tucavaca aulacogen; 7—Phanerozoic sedimentary cover; 8—Pampean magmatic arc. 9—Concealed cratonic areas. See text for details.

covered by extensive Phanerozoic sedimentary sequences. It crops out at the Brazilian border with Bolivia and Paraguay and extends to the south into Paraguayan territory. It is part of a tectonically stable cratonic domain of the Paraguay belt (which was folded and regionally metamorphosed during the Neoproterozoic Brasiliano Orogeny), and is overlain by the mainly carbonate platform covers of the Corumbá and Itapocumi Groups (Almeida, 1965 and 1967; Alvarenga and others, 2000; Boggiani and Alvarenga, 2004).

Almeida (1967) was the first to suggest that the Rio Apa region was a direct link to his "Guaporé Craton," which is the southern part of what is now named the "Amazonian Craton." Regarding the geotectonic setting of southern South America during Neoproterozoic time, two main scenarios must be considered in relation to the Rio Apa cratonic fragment. One scenario, proposed by several authors (Dell'Arco and others, 1982; Alvarenga and Saes, 1992; Kröner and Cordani, 2003) described the Rio Apa as an allochthonous feature, which, during the agglutination of Gondwana, was

attached to the Amazonian Craton along the Neoproterozoic Tucavaca belt, which is considered a suture. The other scenario, proposed by Ruiz and others (2005), and followed by Cordani and others (2009), described the Rio Apa cratonic fragment, in the Neoproterozoic, as a prolongation of the Amazonian Craton. In this case, the Tucavaca belt would correspond to an aulacogenic feature (Ávila-Salinas, 1992) developed over continental crust as a reflection of the compressional tectonic episodes of the Paraguay-Araguaia/Tocantins orogen. Figure 1, adapted from Ruiz and others (2005), illustrates this idea.

The position of the Rio Apa cratonic fragment within the context of the Meso- and Neoproterozoic supercontinents, and consequently its correlation with its neighbouring continental masses, is relevant in order to investigate the tectonic evolution of the Grenvillian mobile belts related to the agglutination of Rodinia and Gondwana. For the terminal Mesoproterozoic, attempts to establish a correlation should be made taking into consideration the tectonic provinces of the Amazonian Craton, as well as the dispersed Grenvillian-type basement inliers within the younger tectonic framework of the Andean Cordillera. Therefore, the determination of its geological history is crucial to put on a better basis its possible position within the context of Rodinia. Moreover, it is also important to understand its role during the agglutination of Gondwana.

A great deal of geochronological information about the Rio Apa cratonic fragment has been available since the first comprehensive geological mapping was carried out (Araujo and others, 1982; Godoi and others, 1999), in which several Rb-Sr and K-Ar determinations were obtained at a reconnaissance scale. As a result, the polymetamorphic character of the region was clearly demonstrated. Later, a series of additional Rb-Sr measurements, plus several Ar-Ar, U-Pb and Sm-Nd ages, were obtained, and many of them were made known as preliminary notes (Cordani and others, 2005a; Cordani and others, 2008a and 2008b). Some additional U-Pb SHRIMP ages and Sm-Nd model ages were also included in the regional report of Lacerda-Filho and others (2006), although in this case the analytical data for the U-Pb ages were not reported. This important set of geochronological data makes it possible to compare and evaluate the interpretative values of different dating methods employed on the same rock samples, which were collected within the same area and belong to the same geological context. We recognize that the existing data falls into three categories: (1)—already published data and interpretations, such as those reported by Araujo and others (1982) and Godoi and others (1999); (2)—data included only in internal reports or other publications not easily accessible outside Brazil; and (3)—completely new data and ideas, as those reported in this work.

The objective of this work is therefore to make a comprehensive report of the geochronological studies conducted in the Rio Apa Craton and produce a consistent interpretation of the tectonic evolution of this unit. In this respect, our objectives are:

(1) to integrate the interpretation of the geochronological data in order to establish the relative sequence of regional tectonic events;
(2) to try to interpret properly the tectonic significance of the apparent ages and isotopic constraints determined by different methods;
(3) to try to correlate the Rio Apa cratonic fragment with the neighbouring tectonic provinces within central South America, in order to suggest a suitable relative position for it in Rodinia and Gondwana; and
(4) to report in the tables and appendices all the pertinent analytical data related to the U-Pb, Rb-Sr, Sm-Nd, K-Ar and Ar-Ar measurements, indicating the source of each age listed.

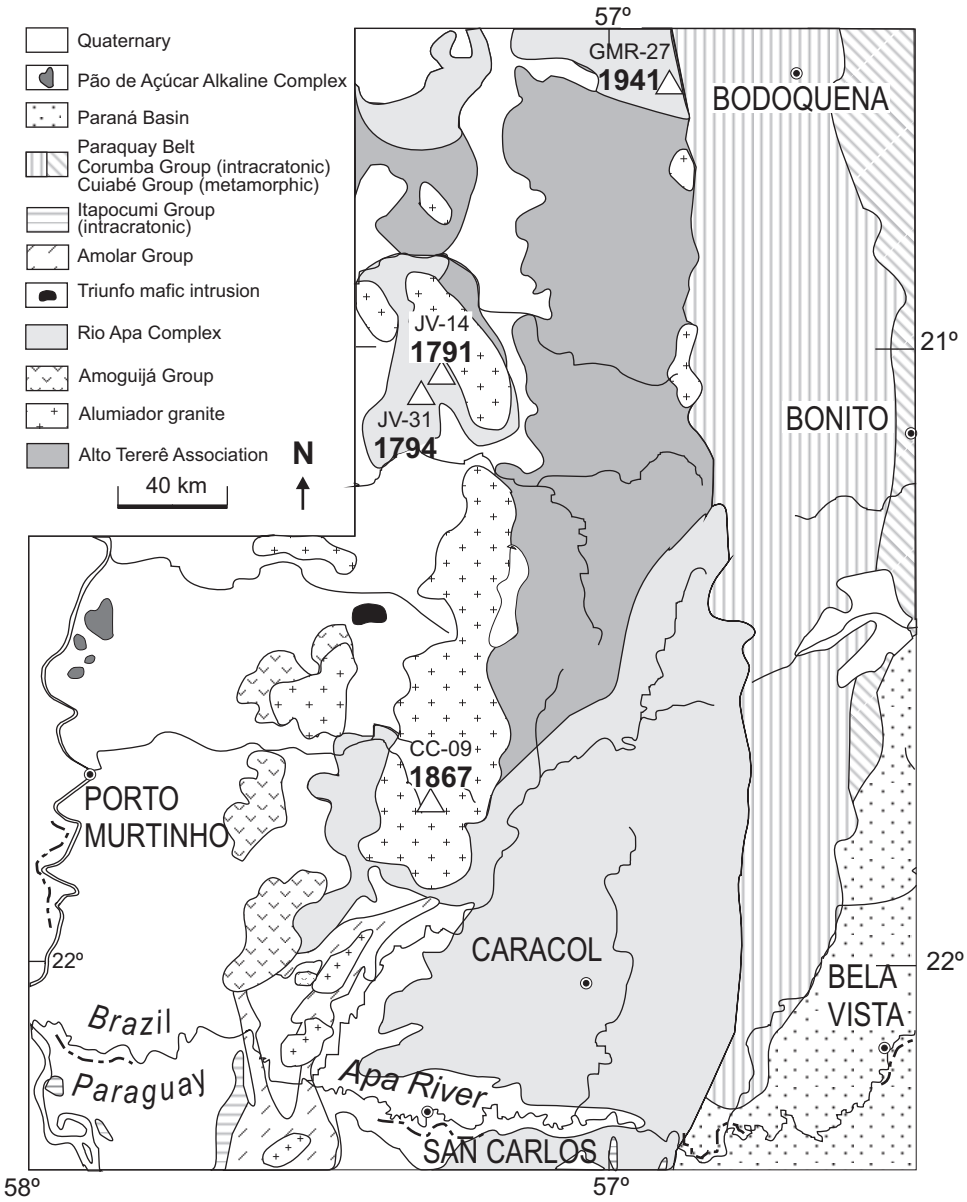

Fig. 2. Geologic outline of the Rio Apa Craton in Brazil. Location of U-Pb SHRIMP zircon ages from Lacerda Filho and others (2006) is shown by open triangles, together with age in Ma.

GEOLOGICAL SETTING

Figure 2 is a regional sketch map of the main area of exposure of the Rio Apa Craton, which is bound to the east by the Paraguay belt, in SW Mato Grosso do Sul, Brazil. This map was adapted from Lacerda-Filho and others (2006). These authors considered all information from the geological maps produced by Araujo and others (1982), Godoi (1999) and Godoi and others (1999), as well as the digital geologic maps (1:1 million scale) published by Delgado and others (2003). In their work, they

presented new structural, geochemical and geochronological data and re-interpreted the regional tectonic evolution. An updated lithostratigraphic column was suggested, and the geodynamic environment for the formation of the main Precambrian geological units was proposed. Their tectonic interpretation was considered in this study as the latest comprehensive and updated situation, prior to the discussion carried out in this paper, which is based on the new isotopic determinations. In this figure, the approximate location of four samples dated by U-Pb SHRIMP in zircon at the Australian National University at Canberra and reported by Lacerda-Filho and others (2006) is shown. Regrettably, the complete analytical data for these dates, including the precision of each age measurement, is not available.

Large parts of the area shown in figure 2 are covered by the recent sediments of the Pantanal Formation and by the Paleozoic sedimentary rocks of the Aquidauana Formation. They will not be discussed here, as well as the Triassic intrusions of the Fecho dos Morros alkaline Complex.

Considering the geotectonic setting at the Precambrian-Cambrian boundary, the Rio Apa Craton stands up as the foreland domain for the Paraguay belt. The basement rocks are overlain by the intracratonic cover of the Corumbá Group along the Serra de Bodoquena in Brazil and the southernmost part of the region. In that stratigraphic unit, carbonate sediments predominate, showing peculiar metazoan fossils (Cloudina, Corumbella werneri), which indicate that their age is close to the Vendian/~Early Cambrian boundary (Boggiani and others, 1993). The Corumbá Group shows a clear tectonic and metamorphic polarity increasing toward the easternmost part of the region, where the low-grade metasedimentary rocks of the Paraguay belt occur as a tectonic feature of the Neoproterozoic Brasiliano Orogeny. Figure 2 shows in its north-eastern corner the low to medium-grade metamorphic rocks of the Cuiabá Group, which is composed predominantly of muscovite schists and quartzites and has NW trending conspicuous structures. These correspond to large fault zones, in which the Cuiabá fold and thrust belt overrides the less metamorphosed sequences of the Corumbá Group. For the older Precambrian units making up the basement rocks in figure 2, the interpretation of their geological history, and especially their structural evolution, is very complicated.

Lacerda-Filho and others (2006) consider the Alto Tererê association, which is composed of supracrustal rocks, to be the oldest unit in the region. It comprises a sequence of low- to medium-grade metavolcano-sedimentary rocks, where muscovite-biotite schists predominate, sometimes with garnet porphyroblasts. Muscovite-biotite gneisses and quartzite intercalations are common. Metabasic rocks also occur in many places. The differential erosion between the schists and the large quartzite intercalations enhances the complicated sinuous structures, which further indicate the complexity of the structure of the Alto Tererê metamorphic terrain. The metabasic rocks are mainly amphibolites with MORB-type chemistry, which were interpreted as remnants of an old Paleoproterozoic oceanic crust. Corrêa and others (1976) named this unit the Alto Tererê Group and this name was retained by Godoi and others (1999) and Lacerda-Filho and others (2006), although with somewhat different geological meanings. In the northeastern part of the area, close to the town of Baía das Garças and very close to the contact with the overlying Corumbá Group, the Alto Tererê schists are intruded by three small, slightly foliated granitic massifs, as shown in figure 2.

Araujo and others (1982) proposed the name "Rio Apa Complex" for a very heterogeneous unit, comprising medium- to high-grade metamorphic rocks and granites and occupying a large area in the central part of the region. The name of this tectono-stratigraphic unit was retained by Lacerda-Filho and others (2006) with the same meaning. In the northern part of the area, in the vicinity of the town of Morraria (fig. 3), banded gneisses and migmatites predominate, with frequent intercalations of

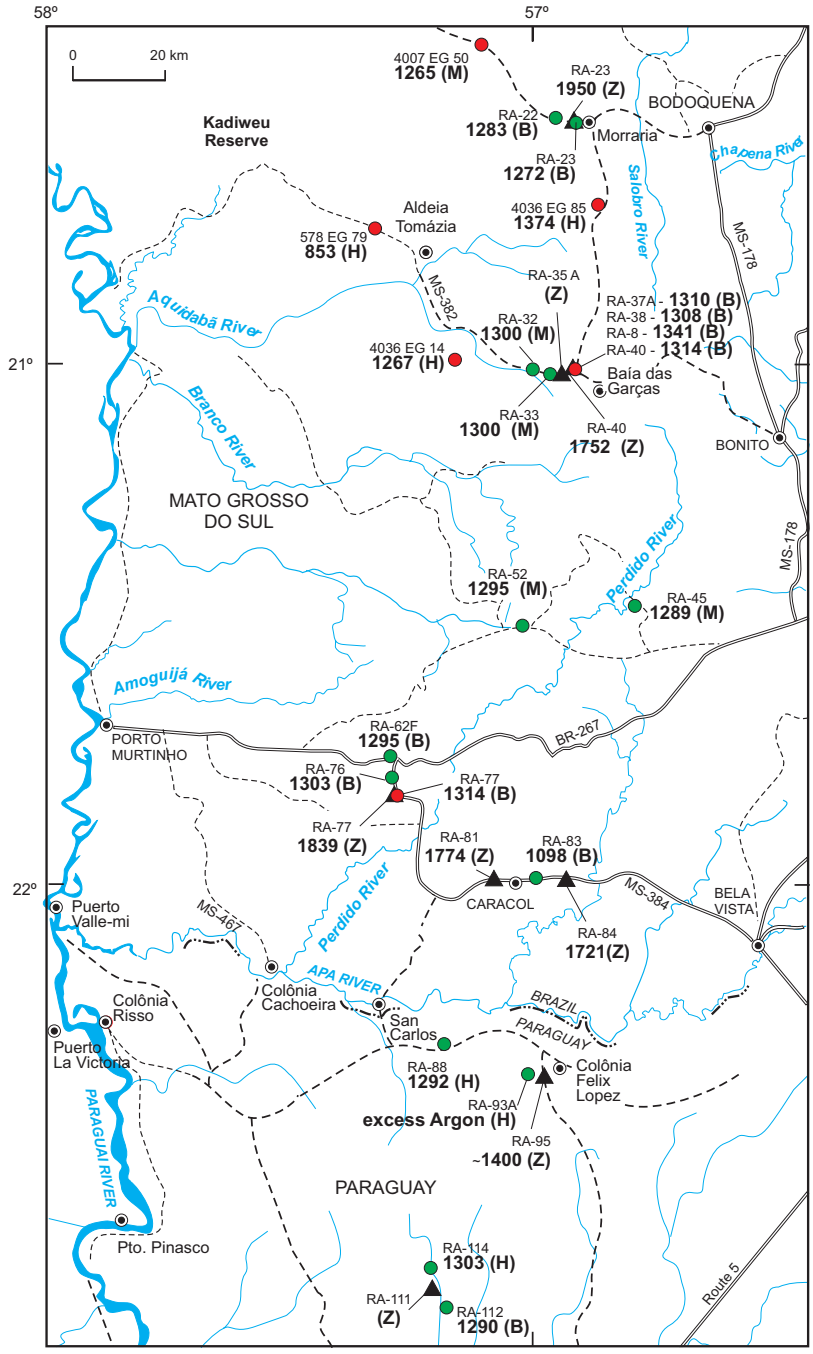

Fig. 3. Location of samples from the Rio Apa Craton dated by U-Pb, K-Ar and $^{40}Ar/^{39}Ar$ methods. Green circles = $^{40}Ar/^{39}Ar$ method; Red circles = K-Ar; B = biotite; M = muscovite; H = hornblende; Z = zircon. Black triangles = U-Pb. Numbers and ages refer to data presented in the tables.

amphibolite. These medium- to high-grade metamorphic rocks were attributed to a series of Paleoproterozoic calc-alkaline magmatic arcs. To the east of the city of Porto Murtinho, banded gneissic rocks also occur. These rocks were considered by Lacerda-Filho and others (2006) as correlative with the northern gneisses located near Morraria. They are covered by the Serra da Bocaina felsic volcanics and intruded by the granitoid rocks of the Alumiador batholith, which contains xenoliths of the banded gneisses.

In the central part of the region, slightly foliated homogeneous orthogneisses are widespread from about the latitude of the town of Bonito to the town of Caracol to the south. These rocks were also included in the Rio Apa Complex by Lacerda-Filho and others (2006), following the previous work of Araujo and others (1982). However, they are quite different from the banded gneisses of the northern and western parts of the region, especially in their paragenesis, which includes very small amounts of mafic minerals. They are essentially orthogneisses, with a very simple mineralogy, composed of quartz, microcline and oligoclase as the main components. Later in this work, the Rio Apa Complex will be divided into three separate litho-stratigraphic units: "the Morraria and Porto Murtinho banded gneisses and the Caracol leucocratic gneisses."

According to Araujo and others (1982) and most subsequent authors, including Lacerda-Filho and others (2006), the Serra da Bocaina volcanics have been considered to be the extrusive equivalent to the Alumiador granites, as components of the Amoguijá Suite. The volcanic rocks include porphyritic rhyolites and dacites, associated with minor pyroclastic rocks and volcanic breccias. The Alumiador batholith takes the form of a large elongated intrusion in the central part of the region, showing conspicuous NNE trending lineaments along the Serra do Alumiador and deflecting to a NW trend along the Serra da Alegria. It is formed essentially of fine- to medium-grained isotropic syeno- to monzogranites, also including some granophyric varieties. A second large portion of the Alumiador suite forms an extension to the north, trending NW and including similar granitic rocks. In this region, the batholith is surrounded and intruded by a gabbro-anorthositic suite, which was named Serra da Alegria, as reported by Silva (ms, 1998), and this name was retained by Lacerda-Filho and others (2006). It is a cumulative magmatic suite, in which anorthosites and leuco-gabbros to mela-gabbros occur, some of them with igneous banding. The gabbroic rocks of the Morro do Triunfo Mafic Intrusive, indicated in figure 2, may be coeval with the Serra da Alegria magmatic rocks. All intrusive granitic bodies occurring in the region were considered correlative with the Alumiador granites mainly because of the lack of geochronological control (Araujo and others, 1982; Godoi and others, 1999; Delgado and others, 2003; Lacerda-Filho and others, 2006). This is the case, for example, for the already mentioned granites intruding into the schists of the Alto Tererê Group in the northeast corner, near Baía das Garças, which will be considered as a separate unit later in this paper.

Near the Brazil-Paraguay border (fig. 2), several outcrops of low- to medium-grade metamorphic sequences were united by Lacerda-Filho and others (2006) under the informal name of "Amolar Domain." They are considered as correlative with the 1.10 to 1.00 Ga Sunsás orogeny of the Amazonian Craton (see fig. 1) and, therefore, are tentatively attributed to the late Mesoproterozoic. A larger area occupied by this unit was identified near the Apa River, entering Paraguay and forming a large zig-zag structure. The main lithologies include different types of supracrustal rocks, among which quartzites and sericite-schists predominate, although meta-volcanic rocks are also present. The rocks of the Amolar domain are intruded by small granitoid plutons. No dating is available yet, either of the supracrustal rocks or the intrusive granites. Therefore, any possibility of correlation is only tentative.

In the case of the territory of Paraguay, the main information was obtained from the reconnaissance geological map produced by the Anchutz Corporation in the 80s and later incorporated by F. Wiens in his Ph. D. dissertation (Wiens, ms, 1986). When the samples used in this study were collected, some observations made by the senior author, in 2003, during field work in the area, were also considered.

In the following comments, we will try to correlate the lithologic and stratigraphic units found in Paraguay with the ones already established in Brazil by Lacerda-Filho and others (2006). It is obvious that the sedimentary rocks of the Paraná Basin are also present at the eastern portion of the Paraguayan region, and it is possible to establish the correlation of a few small outcrops of limestone with the Corumbá Group. The Quaternary cover along the Paraguay River is the same in Brazil and in the western portion of Paraguay. In addition, the metamorphic rocks of the Amolar domain are also present in Paraguay, forming a coherent structure. The Itapocumi stromatolitic limestone, containing minor intercalations of siliciclastic rocks and considered to be correlative with the Corumbá Group, occurs in this area covering the Amolar supracrustals.

In the central part of the area, Wiens (ms, 1986) named as "Paso Bravo Province" a complex and diversified region in which medium-grade metamorphic rocks are predominantly exposed. The western part of this unit, formed by pink to gray, medium- to coarse-grained, strongly foliated granitic gneisses, may easily be considered as the continuation in Paraguay of the Caracol leucocratic gneisses described above and included by Lacerda-Filho and others (2006) in their Rio Apa Complex. On the other hand, the eastern part of Wiens' (ms, 1986) Paso Bravo Province seems not to have a counterpart in Brazil. In that area, there is a predominance of banded gneisses, in which, besides feldspars and quartz, a great deal of mafic minerals are recorded, such as hornblende, biotite, garnet and pyroxene. Migmatites are also described, as well as a few granitic intrusions, formed mainly by massive to weakly foliated, medium to coarse-grained biotite granites, sometimes with muscovite, and locally exhibiting porphyritic texture.

Structural Context

In order to recognize the large-scale regional structures, many observations made on the available outcrops by different authors (for example Araujo and others, 1982; Godoi and others, 1999; Ruiz and others, 2005; Lacerda-Filho and others, 2006; Godoy and others, 2009), and by the present authors, as well as the available SLAR images taken in the 70s and more recent satellite images were considered, and some general ideas on the regional structural evolution can be proposed as follows:

1—As expected, the areas covered by the Quaternary formations and the sedimentary rocks of the Aquidauana Formation and the Corumbá Group are virtually structureless. This also is true for the peneplanized areas of the various granitoid-gneissic terrains in Brazil and Paraguay. Some low crustal-level faults produced by relatively young Phanerozoic tectonics affected the Corumbá and Itapocumi limestones. They are mainly normal, but sometimes can be compressional. Moreover, it is apparent that the Pantanal Formation, including younger alluvium deposits forming swampy terrains, is now subsiding, characterizing one of the initial episodes for the formation of a new large sedimentary basin in central South America.

2—Neoproterozoic tectonics, related to the activity of the Paraguay fold belt, are also at low crustal level. The tectonic polarity of the low-grade metamorphic rocks of the Cuiabá Group towards the cratonic area is evident. Recumbent folds are observed, and the rocks have slaty cleavage and axial plane schistosity. Later deformational phases are also observed, producing crenulation and mylonitic foliation along transpressive zones. Regarding the platform cover of

the Corumbá Group, there is only gentle folding with eastward dips and practically vertical axial planes. The same occurs for the Itapocumi Group in Paraguay, but there is one difference; the gentle dips of this unit are westward directed. Moreover, affecting the Puerto Valle-Mi outcrop of limestones and shales of the Itapocumi Group, along the Paraguay River, Campanha and others (2008) described a series of thrust faults associated with low-grade metamorphism. Regarding the Rio Apa Craton basement rocks, evidence for Neoproterozoic tectonics is barely visible.

3—Considering the basement rocks, a regional foliation can be observed in all the lithological units, especially in the southern part of the area. In the gneisses located near Caracol, it stands up as a penetrative schistosity, often with variable attitudes and possibly related to a pervasive medium-grade metamorphic event. Along the BR 267 highway, these rocks show low dip angles (around 20°) to the SW. In contrast, in the Alumiador suite, a few kilometers to the west along the same highway, a similar structural deformation is observed, showing similar trend but with high dip angles (70-80°) always towards the SW. Farther west, the Serra da Bocaina volcanics have a slaty cleavage with moderate dips to the SW, which may also be related to the same regional deformation.

4—A strong deformational episode can also be observed in the central and northern areas, where different gneissic rocks and the Alto Tererê supracrustal rocks occur. Variable lithologies with quite different rheological properties and also variable structural trends are reported. Often, at least one older deformational phase is detected. Moreover, the strong penetrative and axial plane schistosity, where this can be observed, is practically parallel to bedding, indicating the existence of isoclinal folding.

5—In a coherent structural picture, it is difficult to include in the Amolar metamorphic domain the small and sparse outcrops of low-grade supracrustal rocks present in the northwestern part of the region, as Lacerda-Filho and others (2006) did. This is only possible for the southern structure that crosses the Rio Apa from Brazil to Paraguay. In Brazil, this structure has a NE trend, making up what seems to be an antiform with an inverted flank and axial plane dipping towards the south-east, whose core is filled with small granitic bodies (fig. 2). In Paraguay, the same antiform bends sharply to a NW trend and comes back later to a NE trend, but keeping its internal granites. One of these, a biotite granite, forms a nucleus of what Wiens (ms, 1986) characterized as the "Centurion structural high." This large zig-zag antiform indicates a westward tectonic transport.

GEOCHRONOLOGICAL RESULTS

Dating of the Rio Apa Craton was carried out mainly at the Geochronology Research Center of the University of São Paulo (CPGeo-USP) (K-Ar, Ar-Ar, Rb-Sr and Sm-Nd), using the samples collected in 2003 by the senior author, firstly for the RadamBrazil Project (Araujo and others, 1982) and more recently for this work. The U-Pb ages were obtained at the Beijing SHRIMP Center (China) and some of the Sm-Nd analyses were obtained at the Federal University of Brasilia (Brazil). Preliminary data were presented at a few scientific meetings (Cordani and others, 2005a, 2008a, 2008b), and the abstracts published in these events are mentioned in the references. All available geochronological data for the region will be presented according to the methodology employed and examined and evaluated in terms of the direct interpretative value of each method. The first four tables present the K-Ar, ^{40}Ar-^{39}Ar, Rb-Sr and Sm-Nd determinations, respectively, and the complete analytical data for the U-Pb and ^{40}Ar-^{39}Ar analyses are shown in Appendices 1 and 2, respectively.

Already published data, such as the K-Ar and Rb-Sr measurements reported by Araujo and others (1982), are indicated in the pertinent tables and appendices. However, the data presented at scientific meetings, such as the above mentioned, as well as those only included in internal reports or other publications not easily accessible outside Brazil, will be considered in a similar way as the new data produced for this work.

U-Pb SHRIMP Determinations

U-Pb dating was carried out on single zircon crystals from eight samples, employing the SHRIMP II instrument installed at the Chinese Academy of Geological Sciences and operated from São Paulo using the SHRIMP Remote Operational System (SROS) device. Details of the analytical procedures are presented by Williams (1998). Correction for common Pb was made based on the measured ^{204}Pb, and the typical error component for the ^{206}Pb/^{238}U ratios is less than 2 percent. Uranium abundance and U/Pb ratios were calibrated against the TEM standard. Zircons were extracted from eight samples of granitoid rocks, and the location of these samples is indicated in figure 3. The zircon typologies for the samples prepared at the CPGeo-USP are described below, and the concordia plots of the analytical points are shown in figure 4. Age calculations are based on Isoplot 3.0 Ludwig (2003). Appendix 1 presents the apparent U-Pb ages and the complete analytical data.

Sample RA 23 is a strongly foliated, medium-grained biotite-hornblende gneiss from the northernmost part of the area and belongs to the Morraria gneissic unit, in which plagioclase (45%) predominates over microcline (15%). It also includes quartz (25%), biotite (10%) and hornblende (5%), plus titanite, apatite and epidote. Zircons are mainly 200 to 300 μm long subhedral prismatic crystals with dark oscillatory-zoned cores and thin white low-U rims in the CL images. Appendix I indicates this sample has U contents of 200 to 500 ppm, as well as quite low common ^{206}Pb. In figure 4A, six zircons yield an upper intercept age of 1950 ± 23 Ma (MSWD = 1.06; model 1) [95% confidence]. The three most concordant zircons yielded a weighted mean age of 1935 ± 15 Ma [0.76%] (2σ internal).

Sample RA 77 is an unfoliated pink monzogranite from the Alumiador Suite. Its mineral composition includes plagioclase, microcline and quartz occurring in similar amounts, approximately 30 percent, plus biotite (less than 10%), titanite, zircon, epidote, apatite and opaques. Its texture is equigranular, with millimetric grain size, but including some centimeter-sized K-feldspar crystals. In this sample, large euhedral to subhedral prismatic zircon crystals, 180 to 300 μm long, are found. CL images show oscillatory-zoned cores and dark (possibly magmatic) resorbed borders. The crystals are dark brown and fractured, infilled with high-U zircon. Appendix 1 shows that the U content is variable, usually between 70 to 270 ppm, but with some high-U crystals, up to 773 ppm. In figure 4B, nine analyses yield an upper intercept age of 1839 ± 33 Ma (MSWD = 1.12; model 1) [95% confidence].

Samples RA 35A and RA 40, which were collected near Baía das Garças and have very similar mineral composition and textures, are unfoliated to slightly foliated, pink colored granitic rocks which intruded the Alto Tererê metamorphic rocks. They contain plagioclase (40 to 50%), microcline (about 30%), quartz (20 to 30%) and some biotite. Zircon, allanite, apatite, chlorite and opaque minerals are the common accessories. These rocks are medium grained with magmatic textures. Sample RA 35 consists of euhedral zircon crystals, usually short prisms with pyramidal terminations, 50 to 150 μm long. A smaller population of larger crystals, up to 300 μm long, can also be found in this sample. In the CL images, oscillatory-zoned cores and relatively large dark high-U zircon overgrowths are observed. The U content is mostly between 250 to 550 ppm (Appendix 1), but some zircons show higher contents, up to 2048 ppm. In figure 4C, nearly concordant zircon yield a ^{207}Pb-^{206}Pb age close to 1730 Ma (see Appendix 1), and the other more discordant zircons possibly indicate a multi-

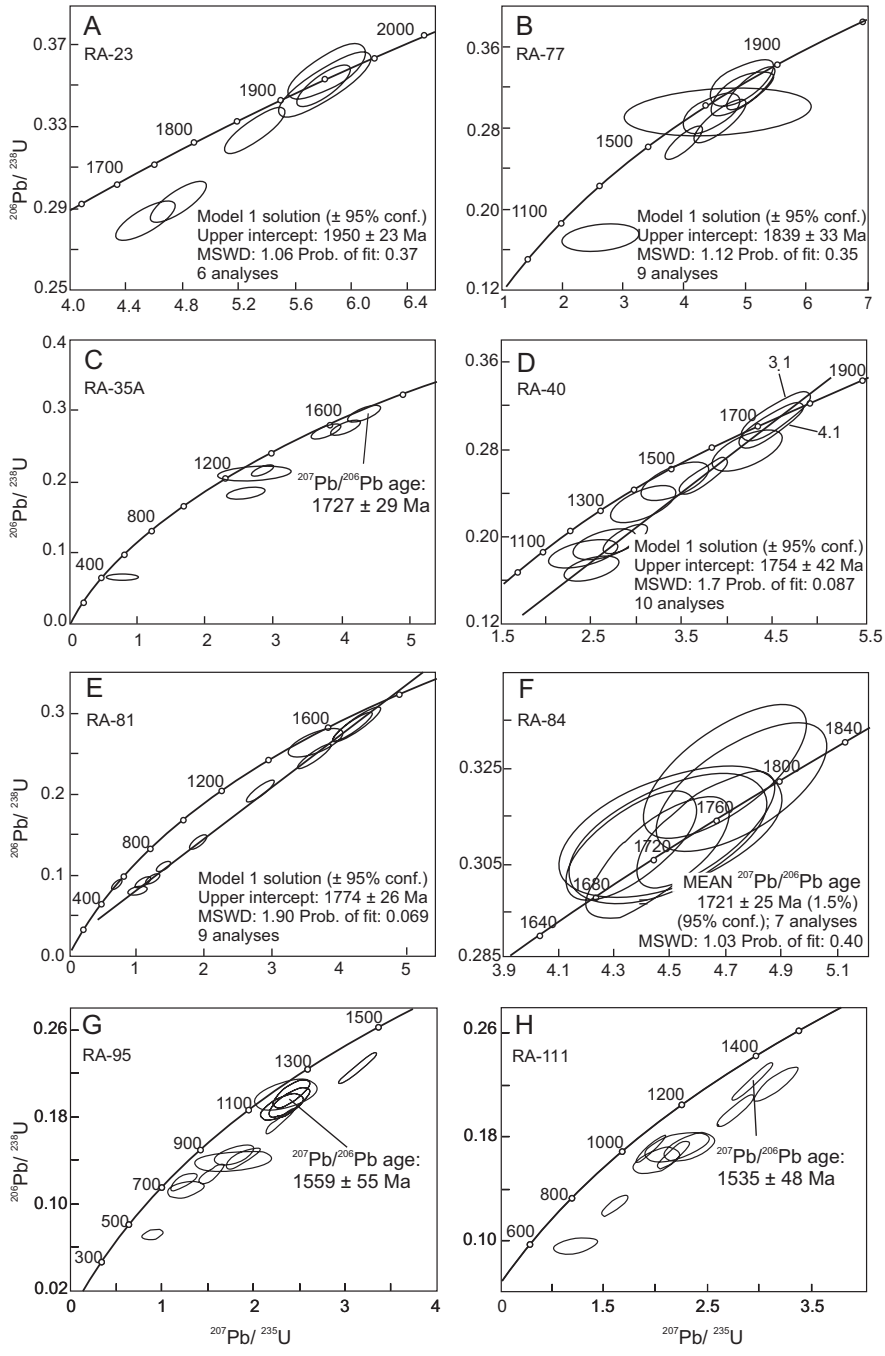

Fig. 4. (A) to (H) Concordia diagrams, showing the analytical points of the U-Pb SHRIMP zircon analyses of rocks from the Rio Apa Craton. Numbers in top left corners are sample numbers discussed in text.

branched pattern of Pb-loss. In sample RA 40, zircons are mainly large subhedral crystals, with pyramidal terminations, and 200 to 300 μm long. They are dark brown and heavy fractured. The CL images are complex, showing oscillatory-zones, but also some sector-zoned cores, together with many oscillatory-zoned overgrowths. Thin dark rims are observed, as well as embayments filled with high-U zircon. The dated zircons have moderate U content of 110 to 320 ppm and usually low common Pb (Appendix 1). In figure 4D, ten zircons yield an upper intercept age of 1754 ± 42 Ma (MSWD = 1.7; model 1), whereas two concordant zircons (#4.1; #3.1) yield a concordia age of 1739 ± 18 Ma (1σ) (MSWD = 0.89). The variably discordant zircons trend toward a lower intercept with a Neoproterozoic age.

Samples RA 81 and RA 84, which were collected near Caracol and have very similar mineral composition, are slightly to moderately foliated, light gray to pink, medium- to high-grade leucocratic orthogneisses. They contain microcline (30-40%), quartz (35-40%), plagioclase (20-25%), and some biotite (usually less than 5%). Zircon, apatite, epidote and opaques are the common accessories. These rocks have a medium grain size, and their textures are always granoblastic. Sample RA 81 includes a population of 80 to 200 μm long subhedral to euhedral prismatic zircons, some of which are rounded and show resorption features. CL images show complex structures with cores of different types, as well as borders and embayments filled with high-U zircon. The U content is very variable, ranging between 150 to 900 ppm (Appendix 1). The U content of one particular zircon crystal was higher than 2000 ppm. Figure 4E shows that nine out of eleven analyses (#6.1 and #9.1 were excluded) determined an upper intercept age of 1774 ± 26 Ma (MSWD = 1.9; model 1). Moreover, one concordant crystal showed a much younger $^{206}Pb/^{238}U$ age of 548 ± 14 Ma, suggesting the possibility of some growth of new zircon during the late Neoproterozoic. Sample RA 84 contains 80 to 150 μm long subhedral to anhedral short prisms. The CL images show light gray cores with igneous zoning and white low-U rims. Appendix 1 shows U content between 90 and 200 ppm and low common Pb. Figure 4F shows that all measured crystals are concordant, with a weighted mean age of 1721 ± 25 Ma (MSWD = 1.03). This age is broadly comparable with that of RA-81.

Samples RA 95 and RA 111, which were collected in Paraguay, are assigned to the Paso Bravo Province of Wiens (ms, 1986). Sample RA 95 is a gray granitoid gneiss, and RA 11 is a pink granite. Both rocks are slightly foliated and contain microcline (about 40%), quartz (35%) and plagioclase (25%), with minor amounts of biotite; zircon, apatite, chlorite and opaque minerals are accessory. Sample RA 95 consists of 150 to 350 μm long fragments of anhedral crystals, many of them rounded and with evidence of resorption. The CL images show complex structures, whose cores are in part sector-zoned and in part made up of magmatic oscillatory-zoned zircon. The crystals have dark borders and many embayments and fractures filled with high-U zircon. The U contents are mostly high but variable. For some grains, the content ranges between 200 to 420 ppm, for others, it ranges between 1100 to 1400 ppm, and for several others it is higher than 2200 ppm (Appendix 1). In several cases, a large common Pb correction was necessary. Sample RA 111 consists mainly of 100 to 220 μm long anhedral crystals and fragments, which are very similar to those of sample RA 95. Most of them are completely dark, with embayments indicating resorption. Like in sample RA 95, U content of the crystals is very high, measuring at least 900 ppm, with some grains up to 2800 ppm (Appendix 1). Figures 4G and 4H show that all crystals from both samples are discordant, showing multi-stage Pb diffusion, dominated by recent Pb-loss. No meaningful age could be determined because of discordance.

In summary, with the exception of samples RA 95 and RA 111, in which all analyzed zircon crystals were variably discordant, the other six samples (figs. 4A to 4F) included at least two concordant or nearly concordant analyses, making possible a

conventional interpretation and attributing the preferred $^{207}Pb/^{206}Pb$ ages to the main episodes of magmatic crystallization of their protoliths. Moreover, considering the presence of a great majority of discordant crystals, and especially the complex multi-stage pattern displayed by the discordia, it is suggested that a series of thermal episodes affected the region, and consequently Pb loss may have occurred at different times.

Regarding samples RA 23 and RA 77, the presence of a few concordant grains made it possible to interpret their age in the conventional way. The age of the former (1935 ± 15 Ma), which was calculated using the weighted mean of all measured $^{207}Pb/^{206}Pb$ ratios, is the first indication of the existence of Paleoproterozoic crust in the evolution of the Rio Apa Craton. On the other hand, the age of sample RA 77 (1839 ± 33 Ma) dates the intrusion of the Alumiador Suite. In both cases, a few discordant points indicate the occurrence of lead loss during later episodes of tectonic evolution. Regarding the Caracol leucocratic orthogneisses of the central-southern region, only in the case of sample RA 84 is a clear indication given about the age of its protolith, which is 1721 ± 25 Ma, calculated using the weighted mean of all seven available $^{207}Pb/^{206}Pb$ analyses. However, a significantly older age was recorded from sample, RA 81, whose nine analyzed crystals provided an upper intercept age of 1774 ± 26 Ma.

Samples RA 35A and RA 40 are of granitic rocks intrusive into the Alto Tererê meta-sedimentary rocks that were collected in the vicinity of Baía das Garças town. For the first, the analytical points in figure 4C are scattered, and the oldest nearly concordant measurement (Appendix 1) yielded a $^{207}Pb/^{206}Pb$ age of 1727 ± 29 Ma. For the second, the regression of the analytical points in figure 4D indicated an upper intercept age of 1754 ± 42 Ma.

Finally, the analytical points of the two southernmost samples, RA 95 and RA 111, assigned to the Paso Bravo Province, are extremely discordant, precluding a reliable upper intercept age. The oldest measured zircon $^{207}Pb/^{206}Pb$ ages can be considered as providing a minimum age for the rocks. For sample RA 95, the oldest $^{207}Pb/^{206}Pb$ age was 1535 ± 48 Ma and for sample RA 111 it was 1559 ± 55 Ma (Appendix 1).

The total number of zircons studied in this work is not sufficient for a statistical evaluation. However, looking carefully at all the diagrams, there is some evidence of possible specific Pb-loss episodes related to regional thermal and/or metamorphic episodes. In a general way, for all of the six dated samples, the scattering related to the discordant points in the concordia diagrams does not indicate a unique trend, but, on the contrary, seems to indicate a multi-branched pattern of Pb diffusion. Moreover, in addition to the possible successive Pb-loss episodes, recent Pb loss can also be suggested, especially in the case of samples RA 95 and RA 111, where the scattering about the discordia trends can be attributed to alteration of metamict zircon crystals.

K-Ar and ^{40}Ar-^{39}Ar Determinations

Table 1 presents seven geologically significant K-Ar determinations performed on rocks of the region. All analyses were obtained at the Geochronological Research Center of the University of São Paulo (CPGeo-USP), four of them during the RadamBrazil Project (Araujo and others, 1982) and three others for the present study. The analytical procedures are described in Amaral and others (1966). Two aliquots from the same sample were used for the K and Ar measurements. Potassium analyses by flame photometry were carried out in duplicate for each pulverized sample. Argon extractions were made in an ultra-high-vacuum system, where a spike of ^{38}Ar was added and the gas was purified in titanium and copper getters. Final argon determinations were carried out in a Reynolds-type gas spectrometer. Analytical precision for K, based on the duplicate analyses, is usually better than 4 percent, whereas for Ar it is

TABLE 1

K-Ar analytical data. See text for details

Sample	Tectonic Unit and Lithology	Rock	Material	%K	^{40}Ar rad ccSTP/g x 10^{-6}	% Atm ^{40}Ar	Age (Ma)
4036/EG-85	Alto Tererê Group	Amphibolite	Amphibole	0.20	16.31	7.3	1374 ± 64
4036/EG-14	Alto Tererê Group	Amphibolite	Amphibole	0.99	71.02	2.5	1267 ± 25
578/EG-79	Alto Tererê Group	Amphibolite	Amphibole	0.32	13.64	3.4	853 ± 58
4007/EG-50	Morraria gneisses	Muscovite schist	Muscovite	8.18	582.20	0.5	1265 ± 14
RA 77	Alumiador batholith	Granite	Biotite	5.49	412.34	1.8	1314 ± 19
RA 38	Baia das Garças granites	Orthogneis	Biotite	6.43	497.15	1.2	1342 ± 20
RA 40	Baia das Garças granites	Granite	Biotite	6.16	462.95	1.8	1315 ± 20

Sample locations are shown in figure 1.

approximately 0.5 percent. Decay constants for age calculation are after Steiger and Jäger (1977).

The location of the analyzed samples is shown in figure 3. In this study, three of the K-Ar ages were obtained from biotite that yielded comparable apparent ages of approximately 1320 Ma. Four others were reported by Araujo and others (1982). One of them, from an amphibole with low K content, yielded a similar apparent age of 1374 ± 64 Ma, but with a large experimental error. One muscovite and another amphibole, with higher K content, yielded apparent ages of 1265 ± 14 and 1267 ± 25 Ma respectively, and a third amphibole (578/EG 79) yielded a much lower apparent age of 853 ± 58 Ma. Although these K-Ar results are not concordant and were affected by large experimental errors, they suggest the occurrence of a Mesoproterozoic regional thermal event at about 1300 Ma.

Fifteen mineral samples were also dated at the CPGeo-USP, using the ^{40}Ar-^{39}Ar method. The determinations were performed using the IEA-R1 nuclear reactor of the Instituto de Pesquisas Nucleares at USP. J values for the irradiated discs were 3.0394 × 10-03 ± 2.87 × 10-06 (SPA-0301-93) and 2.9123 × 10-03 ± 1.78 × 10-06 (SPA-0301-94), respectively. The noble gas purification was obtained in a fully automated ultra-high vacuum extraction line using a 6-W continuous Ar-ion laser and the isotopic ratios were measured on a MAP-215-50 mass spectrometer of the CPGeo-USP. Uncertainties and technical routines of the ^{40}Ar-^{39}Ar dating laboratory are described in Vasconcelos and others (2002).

The step-heating spectra were reported by Cordani and others (2005b), and the complete analytical data can be found in Appendix 2. One of the samples was analyzed only once, eleven were analyzed in duplicate, and three of them in triplicate. The location of the analyzed samples is shown in figure 3, and the age results in table 2.

Table 2 shows that most of the analyses yielded good quality spectra. The tight grouping of very precise plateau ages close to 1300 Ma is the most significant interpretative result, which was obtained from seven biotites and five muscovites. In contrast, biotite RA 83 yielded a significantly younger apparent age of about 1100 Ma. Only one of the measurements, for sample RA 62F, was unsuccessful. However, in the case of the two amphiboles, RA 88C and RA 93A, the spectra were not of good quality, and both measurements showed what appeared to be excess ^{40}Ar.

As already indicated by Cordani and others (2005a and 2008a and 2008b), the ages close to 1300 Ma obtained by both methods, K-Ar and ^{40}Ar/^{39}Ar, were likely associated with a strong and widespread heating event that affected the entire region, with temperatures of at least 350 to 400°C, which are necessary for the complete release of argon from all minerals, including amphiboles. In addition, younger and possibly localized thermal events are suggested by the ages obtained from samples

TABLE 2

*Ar-Ar analytical data (*preferred apparent ages). See Appendix 2 and text for details*

Sample	Mineral	Plateau age, Ma	Integrated age, Ma	Observations
ALTO TERERÊ GROUP				
RA 52	Muscovite	1295* ± 5	1294 ± 3	
		1288 ± 6	1288 ± 6	
RA 32	Muscovite	1300* ± 3	1302 ± 2	
		1299 ± 3	1297 ± 2	
RA 33	Muscovite	1300* ± 4	1300 ± 3	
		1298 ± 5	1297 ± 3	
RA 45	Muscovite	1289* ± 5	1288 ± 4	
		1277 ± 3	1276 ± 2	
MORRARIA BANDED GNEISSES				
RA 22	Muscovite	1283* ± 3	1284 ± 2	
		1281 ± 2	1281 ± 3	
RA 23	Biotite	1272* ± 3	1242 ± 2	
		1271 ± 4	1260 ± 4	Small plateau
ALUMIADOR BATHOLITH				
RA 76	Biotite	1303* ± 4	1292 ± 2	
		1302 ± 3	1296 ± 2	
RA 62F	Biotite	1295* ± 3	1279 ± 2	
		-	1124 ± 2	Irregular spectrum
BAIA DAS GARÇAS GRANITES				
RA 37A	Biotite	1310 ± 3	1294 ± 2	
		1310* ± 3	1303 ± 2	
RA 38	Biotite	1308* ± 5	1303 ± 3	
		1304 ± 5	1301 ± 2	
PASO BRAVO PROVINCE				
RA 88C	Amphibole	1292* ± 10	1321 ± 4	Small plateau, 2 steps
RA 93A	Amphibole	-	2015 ± 13	Excess argon
		-	1529 ± 6	Excess argon
RA 112	Biotite	1290 ± 4	1267 ± 2	
		1295* ± 5	1296 ± 5	
		-	1265 ± 3	Irregular spectrum
RA 114	Biotite	1308* ± 3	1292 ± 2	
		1303 ± 2	1287 ± 2	
		1299 ± 3	1286 ± 2	
CARACOL LEUCOCRATIC GNEISSES				
RA 83	Biotite	1132* ± 3	1104 ± 2	
		1098 ± 3	1098 ± 3	
		1079 ± 4	1089 ± 2	

Sample localities are shown in figure 3.

578/EG–79 (840 Ma) and RA 83 (1100 Ma), whose tectonic significance should be investigated further.

Rb-Sr Determinations

All fifty-two whole-rock Rb-Sr determinations were obtained at the CPGeo-USP from the Rio Apa Craton. Half of them were already reported by Araujo and others (1982) and are re-discussed in this work together with the new Rb-Sr results. The location of the analyzed samples is shown in figure 5. Analytical procedures were the same for the two sets of analyses and are described in Tassinari and others (1996a). Rb

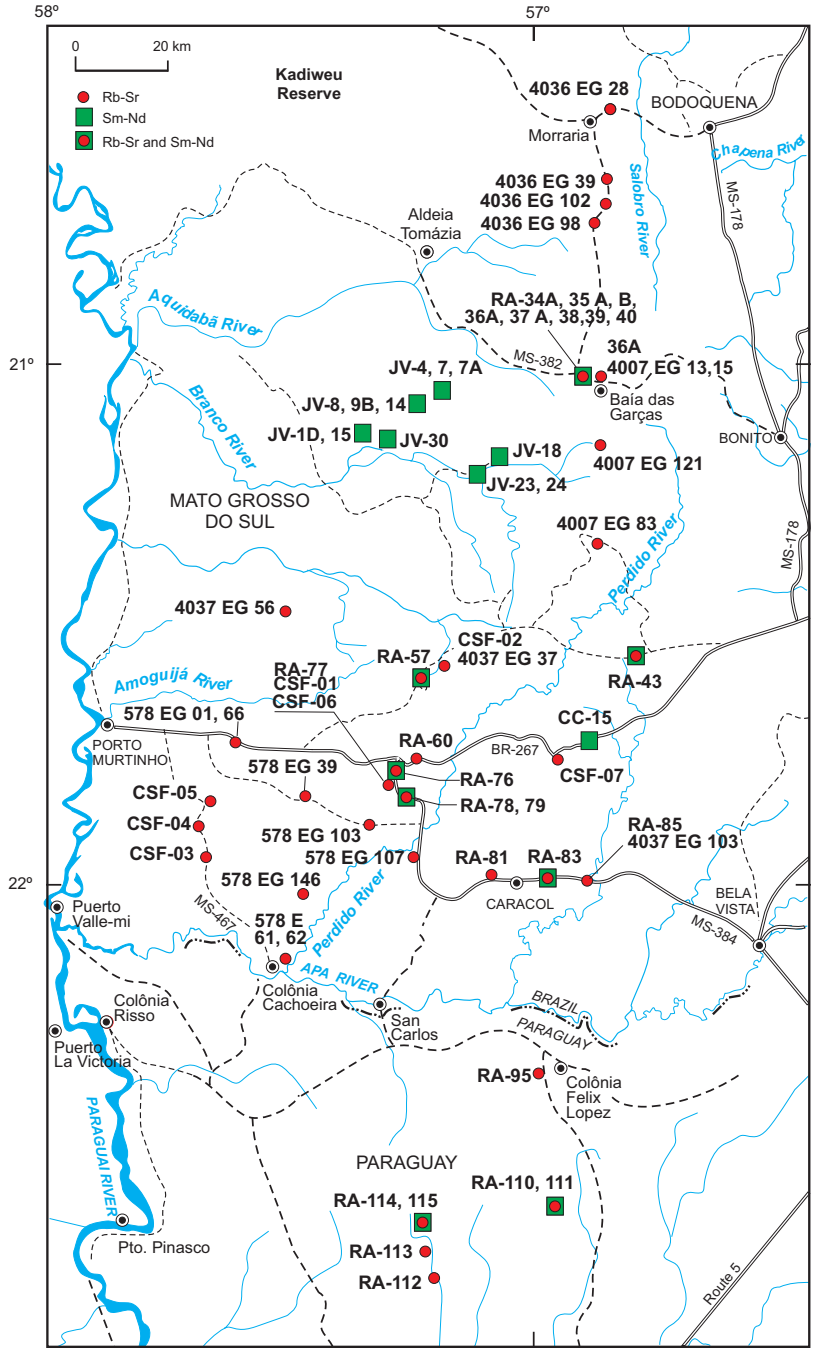

Fig. 5. Location of samples from the Rio Apa Craton analyzed by Rb-Sr and Sm-Nd whole-rock methods. Data summarized in tables 3 and 4.

and Sr values were obtained by either X-ray fluorescence or isotope dilution, when they were below critical levels. $^{87}Sr/^{86}Sr$ ratios were measured with a Finnegan TH5 (the first set) or a Micromass VG-sector (the more recent set) mass spectrometers, and the isotopic ratios were corrected for isotopic fractionation during thermal ionization with $^{87}Sr/^{86}Sr = 0.1194$. Normal precision of the measurements is better than 2 percent for the Rb/Sr ratio and better than 0.01 percent for the $^{87}Sr/^{86}Sr$ ratio. The analytical results are presented in table 3, whose data were used to produce figure 6. Table 3 shows the analytical error for the more recent set is one order of magnitude better than the previous one. Table 3 also includes the calculated Rb-Sr ages, assuming a $^{87}Sr/^{86}Sr$ initial ratio of 0.705, for those samples with high $^{87}Rb/^{86}Sr$ ratio above 4.0, that can be only slightly affected by possible differences from their true Sr initial ratios.

A few measurements were obtained from felsic volcanic rocks, but the great majority were performed on granitoid and gneissic rocks. Because they were collected from different outcrops, the samples cannot be considered cogenetic material. Therefore, the best-fit lines calculated using different regressions are not real isochrons, and the calculated ages can only be used as a reference. Nevertheless, in an exercise in which all 52 analytical points were plotted in the same Rb-Sr correlation diagram, they seemed to be, with a few exceptions, remarkably aligned. The calculated best-fit line showed a slope that would correspond to a reference isochron of about 1700 Ma, with a $^{87}Sr/^{86}Sr$ initial ratio of about 0.706. Cordani and others (2005a) had already commented upon this surprising outcome, because of the large area of the study and the lithological and chemical diversity of the samples. These authors interpreted the resulting age as representative of a widespread medium- to high-grade metamorphism, which produced a pervasive Sr isotopic homogenization that affected all lithological units in the entire region. Only a few samples, notably collected in Paraguay, clearly plotted above the reference isochron. A few others, especially the felsic volcanic rocks, plotted below it, and yielded younger calculated apparent ages.

The samples collected by us (labeled RA) were classified by rock type and tectonic unit. This classification, which was based on the geological setting, as well as on the petrographic and deformational features, is also shown in table 3. The samples collected for the RadamBrasil Project in the 70s were classified by the lithology indicated in Araujo and others (1982), as well as by their location in the region. For many of the dated samples, the content of Rb is higher than 200 ppm and the Sr content is lower than 40 ppm. Samples with high Rb/Sr ratios are found in all geological units, with the exception of the Morraria and Porto Murtinho gneisses. A granitic sample collected in Paraguay yielded the oldest value, 1835 Ma, while the youngest apparent age, 1436 Ma, was obtained from a granophyre associated with the Alumiador intrusive body. Moreover, most of these apparent ages in high Rb/Sr samples fall within the 1600 to 1800 Ma interval. Very high $^{87}Rb/^{86}Sr$ values are always considered suspicious because of the different behavior of Rb and Sr in geochemical processes and their different element mobility. However, the bulk of the collection already indicates the geochemical character of the entire region, where felsic magmatic rocks, usually rich in potassium, are predominant. Lacerda Filho and others (2006) considered both their Rio Apa and Amoguijá tectonic units as related to magmatic rocks. The first includes our Caracol leucocratic gneisses, and the second includes the Alumiador granites and Serra da Bocaina volcanics.

Figures 6A to 6D illustrate the Rb-Sr isochron diagrams that were drawn considering reasonably coherent systems, possibly affected by the same episode of Sr homogenization mentioned above. The samples used to draw the diagrams belong to the same tectonic units and were collected within reasonably short distances from each other (fig. 5). These samples comprise the granitic rocks collected in Paraguay, the Caracol leucogneisses, the Alumiador granite, and the granitoid rocks located near Baía das

TABLE 3

Rb-Sr whole-rock analytical data. See text for details

Sample	Rock Type and Tectonic Unit	Rb (ppm)	Sr (ppm)	$\frac{Rb^{87}}{Sr^{86}}$	$\frac{Sr^{87}}{Sr^{86}}$	T(Ma) (R_i=0.705*)
	PORTO MURTINHO BANDED GNEISS					
578 EG 39*	Biotite gneiss	105.4	457.1	0.67	0.7232	-
	MORRARIA BANDED GNEISS					
4036 EG 8*	Biotite gneiss	145.2	77.2	5.51	0.8355	1650
	ALUMIADOR GRANITIC SUITE					
RA-57	Pink Granite	225.0	72.9	9.118	0.92340	1670
RA-60	Isotropic Granite	205.4	35.5	17.417	1.11996	1660
RA-76	Isotropic Granite	170.0	180.6	2.743	0.77607	-
RA-77	Isotropic Granite	220.4	104.7	6.185	0.85891	1730
RA-78	Foliated Granitoid	354.6	19.5	60.260	2.21426	1740
RA-79	Pink, isotropic Granite	342.9	40.6	25.970	1.34147	1705
CSF 01*	Granite	190.4	86.4	6.41	0.8555	1630
CSF 02*	Granite	219.0	39.9	16.45	1.1030	1680
CSF 06*	Granite	229.3	85.9	7.87	0.8959	1690
578 EG 61*	Granophyre	210.5	63.6	9.77	0.9063	1440
578 EG 62*	Granophyre	211.1	41.9	15.03	1.0250	1480
578 EG 103*	Granite	380.6	24.7	49.19	1.7560	1490
4037 EG 37*	Porphyritic Granite	237.0	53.9	13.10	1.0060	1600
	BAÍA DAS GARÇAS GRANITOID ROCKS					
RA-34A	Pink Granite	325.9	51.0	19.262	1.13885	1570
RA-35A	Pink Granite	314.0	23.9	41.490	1.65382	1590
RA-35B	Aplitic Granite	281.4	24.6	35.748	1.54456	1630
RA-36A	Pink Granite	314.6	19.4	52.987	2.00105	1700
RA-36B	Pink Granite	387.3	22.1	57.754	2.10557	1690
RA-37A	Pink-grey Granite	331.6	50.3	19.924	1.16302	1600
RA-38	Grey Orthogneiss	212.6	315.5	1.959	0.75437	-
RA-39	Pink Aplitic Granite	249.7	22.1	35.487	1.56161	1680
RA-40	Granite	260.3	47.6	16.412	1.08913	1630
4007 EG 13*	Biotite Granite	276.1	45.6	18.23	1.1150	1570
4007 EG 15*	Gneiss	222.8	289.9	2.24	0.7600	-
4007 EG 121*	Gneiss	207.8	190.2	3.18	0.7812	-
4036 EG 39*	Gneiss	221.0	27.2	24.82	1.2780	1610
4036 EG 98*	Gneiss	97.7	297.9	0.95	0.7285	-
EG 102*	Granite	143.1	186.0	2.24	0.7572	-
	SERRA DA BOCAINA VOLCANICS					
CSF 03*	Quartz porphyry	98.6	82.1	3.50	0.7871	-
CSF 04*	Volcanic breccia	113.8	72.3	4.60	0.8045	1510
EG 56*	Rhyolite	139.9	82.1	4.99	0.8207	1615
CSF 05*	Volcanic breccia	139.2	37.1	28.39	1.4160	1740
EG 146*	Rhyolite	413.4	28.7	45.58	1.7480	1590
EG 01*	Rhyolite	133.4	89.7	4.35	0.8097	1670
EG 66*	Rhyolite	238.6	34.5	21.60	1.1510	1440
	PASO BRAVO GRANITOID ROCKS					
RA-95	Granitoid Gneiss	201.5	77.6	7.654	0.89748	1750
RA-110	Pink Granite	187.5	128.2	4.280	0.81705	1820
RA-111	Fine-grained Pink Granite	281.9	41.5	20.723	1.25208	1835
RA-112	Pink Biotite Granite	345.8	35.9	29.918	1.44879	1730
RA-113	Pink Granite	269.5	28.3	29.647	1.48343	1825
RA-114	Porphyritic Granite	176.7	287.2	1.788	0.74947	-
RA-115	Porphyritic Granite	158.2	286.5	1.604	0.74580	-
	CARACOL LEUCOCRATIC GNEISSES					
RA-43	Pink Granite	211.2	30.6	20.977	1.21575	1690
RA-81	Leucocratic Gneiss	220.1	14.6	48.698	1.88942	1690
RA-83	Leucocratic Gneiss	172.7	150.9	3.339	0.79020	-
RA-85	Leucocratic Gneiss	277.0	75.4	10.879	0.93436	1470
558 EG 107*	Granite	238.0	75.7	9.30	0.9340	1710
4007 EG 83*	Monzonite	230.3	259.0	2.59	0.7722	-
EG 103*	Granitic Gneiss	314.5	78.5	11.92	0.9932	1680
CSF 07*	Granite	173.4	55.6	9.23	0.9306	1700

* Samples analyzed for the RadamBrasil Project in the 1970s. Sample localities are shown in figure 5.

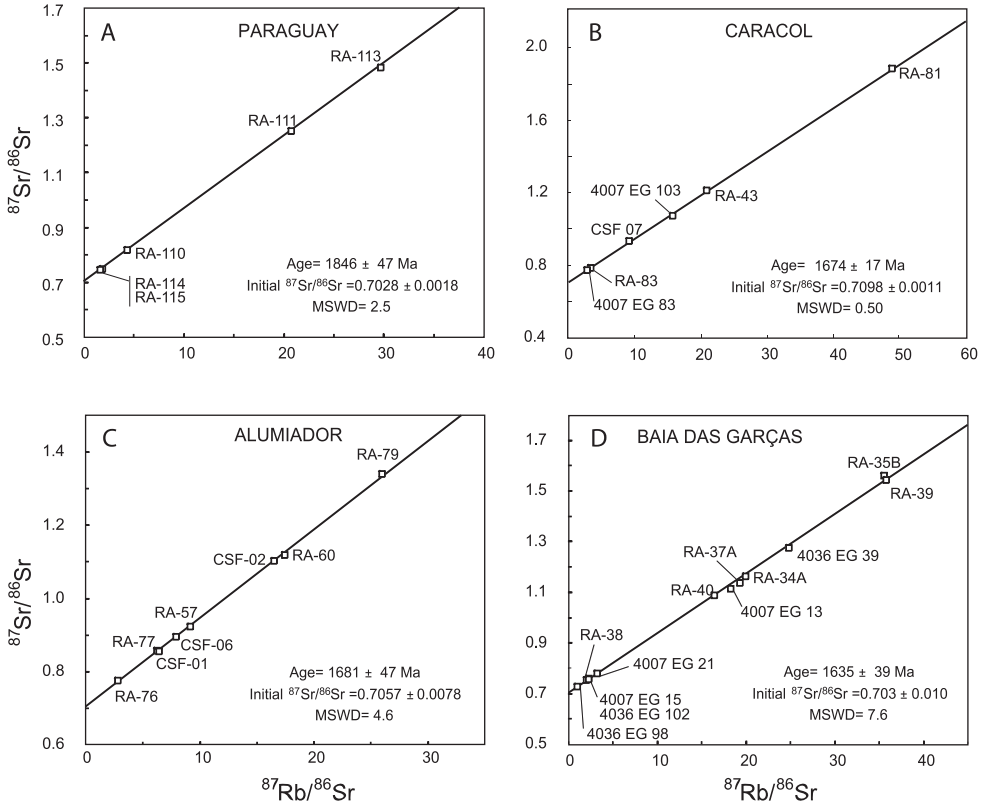

Fig. 6. (A) to (D) Rb-Sr whole-rock isochron diagrams for samples from the Rio Apa Craton, subdivided into Paraguay (A), Caracol (B), Alumiador (C), and Baía das Garças (D). Data summarized in table 3.

Garças and closely associated to the Alto Tererê metamorphics. It should be borne in mind that such classifications may be biased, because many of the samples have mixed character, especially those of the foliated felsic granitoid gneisses, which can belong to more than one category.

Since only two samples from the Morraria gneisses were analyzed, the drawing of a Rb-Sr isochron diagram was not attempted. One of the samples, a banded gneiss (4036 EG 28, location on fig. 5), yielded a calculated age of 1650 Ma (table 3). However, a U-Pb zircon age of 1950 ± 23 Ma, which is related to the magmatic crystallization of the zircons, was obtained from a sample in the same area (fig. 4A).

The felsic volcanic rocks of the Serra da Bocaina Group, all dated by Araujo and others (1982), yielded varied and often much younger calculated apparent ages between 1440 and 1740 Ma (see table 3). Araujo and others (1982) reported a Rb-Sr errorchron for these samples with an apparent age of 1650 Ma. A U-Pb SHRIMP zircon age of 1794 Ma was reported for a volcanic rock attributed to the Serra da Bocaina Group, which was collected in the central part of the area (JV-31 in fig. 2).

The analytical points of five granitic samples collected in Paraguay, corresponding to the granitoid rocks of the Paso Bravo Province of Wiens (ms, 1986), plotted close to the best fit line of figure 6A, whose slope would correspond to an age of 1846 ± 47 Ma, with a low $^{87}Sr/^{86}Sr$ initial ratio of 0.7028. Because of the very low Sr initial ratio, we suggest that this age can be attributed to the magmatic formation of these granitic

rocks. Sample RA 112, also from Paraguay, yielded a somewhat younger Rb-Sr age of about 1730 Ma (table 3). Regrettably, the attempt to determine the U-Pb zircon age for that region (RA 95 and RA 111) was not successful due to the high U content of the zircons, which were affected by strong Pb loss.

Seven samples of granitoid rocks that belong to the Caracol leucogneisses yielded a best fit line corresponding to a calculated age of 1674 ± 17 Ma (fig. 6B), with a $^{87}Sr/^{86}Sr$ initial ratio of 0.7098. This value is very likely related to the pervasive Sr isotopic homogenization episode, which is associated with the medium- to high-grade metamorphic episode, responsible for the granoblastic texture shown by these rocks. Two U-Pb SHRIMP zircon ages are reported for samples of this unit (RA 81 and RA 84; 1774 ± 26 and 1721 ± 25 Ma, respectively) and they probably relate to the igneous formation, within a magmatic arc environment, of the protoliths of these leucocratic gneisses. Therefore, the Rb-Sr isochron age should be related to the regional metamorphism that affected the unit.

Eight samples from the main outcrop of the Alumiador Granite plot close to the best fit line of figure 6C, corresponding to a calculated age of 1681 ± 47 Ma, with a $^{87}Sr/^{86}Sr$ initial ratio of 0.7057. This Rb-Sr age is comparable to the one obtained for the Caracol gneisses, but with a lower Sr initial ratio. According to our interpretation, since the Alumiador granite was affected by strong ductile deformation, this age is tentatively attributed to the same pervasive regional deformational episode. This Rb-Sr isochron age contrasts with the magmatic age of the Alumiador Granite that was obtained by good quality U-Pb data at 1839 ± 33 Ma (see fig. 4B). Two samples of potassic granites and two of granophyres yielded much younger calculated Rb-Sr ages, below 1500 Ma (table 3).

Several samples of granitoid rocks collected from a small area along the MS 382 regional road and close to the locality of Baía das Garças (see fig. 5), not more than a few hundred meters from each other, may be possibly considered cogenetic. They were analyzed by the Rb-Sr and Sm-Nd methods to check their possible correlation with the Alumiador granite and also to investigate the geological history of the Alto Tererê metamorphic rocks, with which they are associated. Twelve samples were analyzed by the Rb-Sr method and the results were included in the diagram of figure 6D, together with the results from three other samples collected from a similar granitic body located about 40 km to the north. One of these granitoid rocks yielded a U-Pb zircon age of 1754 ± 42 Ma (RA 40, see fig. 4 D). The calculated best-fit line in the diagram of figure 6D corresponds to an age of 1635 ± 39 Ma, with a low $^{87}Sr/^{86}Sr$ initial ratio of 0.703. Three samples, all of them with high Rb/Sr ratios, were excluded from the calculations of the best-fit line. When calculated with a $^{87}Sr/^{86}Sr$ initial ratio of 0.705, one of them (RA 35A) yielded an apparent age of about 1600 Ma, and two others (RA 36A and 36B) yielded apparent ages slightly younger than 1700 Ma (table 3).

In summary, the quite reasonable Rb-Sr reference isochrons obtained from three of the four groupings (Alumiador, Caracol and Baía das Garças) seem to be geologically interpretable. However, because each calculation has high errors, the age values should be taken with caution. It is difficult to consider that the calculated ages related to the best-fit lines are different from each other. The three apparent ages, 1674 ± 17 Ma, 1681 ± 47 Ma and 1635 ± 39 Ma, are well within the indicated errors, and perhaps only the 1635 Ma age may be indicating a slightly younger event. For the tectonic interpretations employed in this work, we consider the existence of strong regional metamorphism, at medium- to high-grade, and with an age not far from 1680 Ma, was responsible for quite pervasive Sr isotopic homogenization. The granitoid rocks from Paraguay were possibly formed at approximately 1850 Ma and seem not to be affected by the strong Sr isotopic homogenization observed in the other rocks.

Sm-Nd Determinations

Cordani and others (2005a) reported the first six Sm-Nd whole-rock determinations from the Rio Apa Craton obtained at the CPGeo-USP. Later, nine others were obtained for this study in the same laboratory, using samples of granitoid rocks collected near Baía das Garças. Thirteen additional analyses were made at the Federal University of Brasilia and published by Lacerda-Filho and others (2006). Most of these analyses were conducted on samples from the northern part of the area. The procedures at the CPGeo-USP followed Sato and others (1995). The $^{143}Nd/^{144}Nd$ isotopic ratios were obtained using a multi-collector mass spectrometer Finnegan MAT, with analytical precision of 0.0014 percent (2σ). Experimental error for the $^{147}Sm/^{144}Nd$ ratios is of the order of 0.1 percent. La Jolla and BCR-1 standards yielded $^{143}Nd/^{144}Nd = 0.511849 \pm 0.000025$ (1σ) and 0.512662 ± 0.000027 (1σ), respectively, during the period in which the analyses were performed. $\varepsilon_{Nd(T)}$ values were calculated according to De Paolo (1981), and the constants used include $^{143}Nd/^{144}Nd$ (CHUR) = 0.512638 and $^{147}Sm/^{144}Nd\ (CHUR)_0 = 0.1967$. The Sm-Nd analytical data acquired at the University of Brasilia are only partially available, and their overall precision is similar to that of the USP.

Therefore, a total of 28 Sm-Nd determinations were available to be used in this work. The location of the samples in question (many of them also analyzed by the Rb-Sr method) is shown in figure 5. The critical isotopic data are included in table 4, in which we used the same classification of the geological units used in table 3. Among the relevant analytical data, table 4 shows the calculated Sm-Nd T_{DM} model ages and the $f_{Sm/Nd}$ values. In addition, it also shows the $\varepsilon_{Nd(T)}$ values calculated for the estimated age of the protolith of the rock unit, taken from the available U-Pb SHRIMP zircon determinations, as follows: 1950 Ma for the Morraria gneisses; 1840 Ma for the Alumiador Suite and the Paso Bravo Province; 1800 Ma for the Serra da Bocaina volcanics and the Serra da Alegria magmatic suite, and 1750 Ma for the Caracol leucocratic gneisses and the granitoid rocks near Baía das Garças.

As shown in table 4, the Sm-Nd T_{DM} model ages are grouped in three coherent clusters:

1—The oldest one includes the Alumiador granites, the Serra da Alegria magmatic suite and samples JV 1D and JV 15, located near Serra da Alegria and here attributed to the Porto Murtinho banded gneisses. These samples yield a late Archean average Sm-Nd T_{DM} model age of 2.52 Ga.

2—A second group includes the Caracol leucocratic gneisses, one sample of the Serra da Bocaina felsic volcanics and a few gneissic rocks (JV 18, JV 23 and JV 24) associated with the Alto Tererê schist. Those samples yield a mean Sm-Nd T_{DM} model age of 2.23 Ga. Two granitoid rocks from the Paso Bravo Province of Paraguay also showed model ages close to ages of this group.

3—The youngest group includes most of the granitic rocks of the Baía das Garças, which yield an average Sm-Nd T_{DM} model age of 2.02 Ga. Two exceptions must be noted: sample RA 39, which yielded a slightly older model age, and sample RA 36 B, which yielded the oldest model age of the entire set, 2.81 Ga. Moreover, when considering the Sm-Nd analyses, sample RA 43, which was included together with the Caracol gneisses in table 4, showed, on the contrary, strong affinity with the Baía das Garças granitic rocks.

Figure 7 is a Sm-Nd correlation diagram in which all analytical points are plotted. Since the samples are not cogenetic, good quality and precise isochrons should not be expected. However, the diagram shows that the magmatic history of the rocks has produced significant fractionation between Sm and Nd, and a reasonable correlation enveloping all samples may be observed. Three coherent alignments are shown by different colors in this figure. Each of them represents one of the groupings defined in

TABLE 4

Sm/Nd whole rock analytical data. See text for details

Sample	Rock	Sm (ppm)	Nd (ppm)	$\frac{^{147}Sm}{^{144}Nd}$	$\frac{^{143}Nd}{^{144}Nd}$	$f_{Sm/Nd}$	TDM Ga	Preferred age (t) (Ma)	
ALTO TERERÊ GROUP									
JV 18*	Gneiss	13.225	71.429	0.1119	0.511567	-0.43	2.20	+0.09	1950
JV 23*	Gneiss	4.540	18.793	0.1461	0.512037	-0.26	2.26	+0.80	1950
JV 24*	Gneiss	3.405	13.122	0.1569	0.512189	-0.20	2.28	+1.09	1950
PORTO MURTINHO BANDED GNEISSES									
JV 15*	Gneiss	8.860	51.350	0.1043	0.511224	-0.47	2.53	-4.72	1950
JV 30*	Granite	3.245	19.633	0.0990	0.511414	-0.49	2.17	+0.08	1950
JV 1D*	Gneiss	5.011	31.760	0.0954	0.511047	-0.51	2.57	-5.97	1950
ALUMIADOR GRANITE BATHOLITH									
RA 57	Granite	23.384	109.424	0.1292	0.511650	-0.34	2.53	-3.34	1840
RA 76	Granite	4.415	23.360	0.1143	0.511426	-0.42	2.49	-4.20	1840
RA 78	Leuc. gneiss	1.526	9.329	0.0989	0.511152	-0.50	2.53	-5.91	1840
JV 7*	Granophyre	10.310	50.117	0.1243	0.511639	-0.37	2.38	-2.86	1800
JV 7A*	Granophyre	8.587	38.968	0.1332	0.511680	-0.32	2.58	-4.11	1800
BAIA DAS GARÇAS GRANITES									
RA 34A	Leuc. gneiss	5.289	27.402	0.1167	0.511724	-0.41	2.07	+0.03	1750
RA 35B	Granite	3.571	24.801	0.0871	0.511419	-0.56	1.96	+0.69	1750
RA 35A	Leuc. gneiss	3.251	20.788	0.0946	0.511464	-0.52	2.02	-0.11	1750
RA 36B	Granite	2.584	10.757	0.1452	0.511795	-0.26	2.81	-4.95	1750
RA 37A	Leuc. gneiss	5.107	26.760	0.1154	0.511731	-0.41	2.04	+0.46	1750
RA 38	Orthogneiss	5.757	33.074	0.1053	0.511582	-0.46	2.06	-0.20	1750
RA 39	Leuc. gneiss	3.566	20.098	0.1073	0.511553	-0.45	2.14	-1.21	1750
RA 40	Leuc. gneiss	8.710	43.074	0.1223	0.511831	-0.38	2.02	+0.87	1750
SERRA DA BOCAINA VOLCANICS									
JV 4*	Rhyodacite	11.917	63.139	0.1141	0.511561	-0.42	2.26	-2.04	1800
PASO BRAVO PROVINCE									
RA 111	Leuc. gneiss	2.862	12.555	0.1379	0.511869	-0.30	2.37	-1.13	1840
RA 114	Porph. granite	7.990	41.311	0.1170	0.511648	-0.41	2.20	-0.50	1840
CARACOL LEUCOCRATIC GNEISSES									
RA 83	Leuc. gneiss	7.341	38.704	0.1147	0.511600	-0.42	2.23	-1.94	1750
CC 15*	Leuc. gneiss	25.171	129.760	0.1173	0.511632	-0.40	2.22	-1.90	1750
RA 43	Granite	9.775	56.420	0.1048	0.511636	-0.47	1.97	+0.97	1750
SERRA DA ALEGRIA MAGMATIC SUITE									
JV 8*	Anorthosite	2.230	9.192	0.1468	0.511886	-0.25	2.64	-3.21	1800
JV 9B*	Anorthosite	2.180	9.586	0.1375	0.511792	-0.30	2.50	-2.91	1800
JV 14*	Anorthosite	0.680	3.330	0.1250	0.511573	-0.36	2.50	-4.31	1800

* Samples analyzed at the Federal University of Brasília and reported by Lacerda-Filho and others (2006). Sample localities are in figure 5.

table 4, thus making it possible to offer a tentative explanation in terms of age and geological evolution.

In figure 7, samples JV-1D and JV-15, attributed to the Porto Murtinho banded gneisses, together with three samples of the Alumiador granitic suite and a few samples from the Serra da Alegria magmatic suite (blue color in fig. 7), plot close to a reference isochron of late Archean age. For these rocks, the values of $\varepsilon_{Nd(T)}$ are always negative, up to (−6), suggesting some crustal reworking within the original magma chambers. In contrast, most samples of granitoid rocks occurring near Baía das Garças (red color in fig. 7) are reasonably aligned along a much younger reference isochron of Paleoproterozoic age. Their $\varepsilon_{Nd(T)}$ values are slightly positive, suggesting a predominant contribution of juvenile sources. Two exceptions are noted, samples RA 39 and RA 36B, which yielded negative $\varepsilon_{Nd(T)}$ values, but these samples are the ones that were not aligned with the remaining granitoid rocks of Baía das Garças in figure 7. In

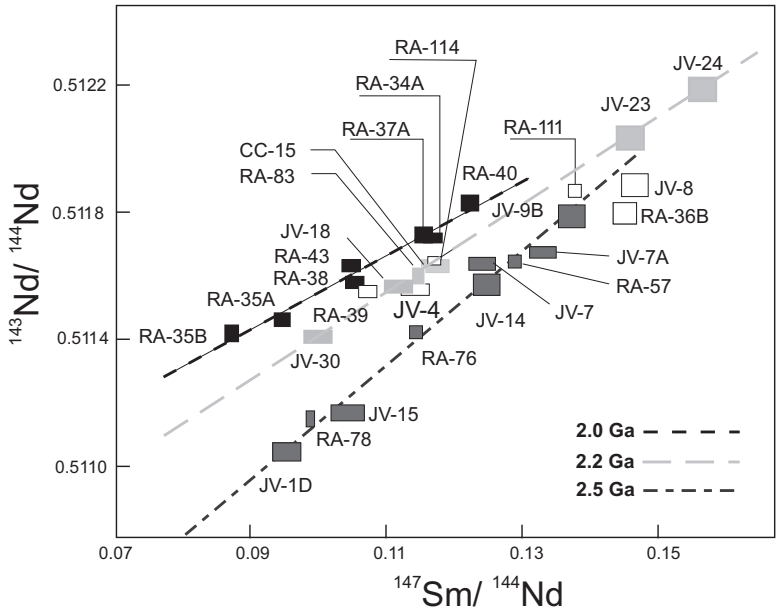

Fig. 7. Sm-Nd correlation diagram for all samples from the Rio Apa Craton. Data summarized in table 4.

between these two reference lines, a few samples scatter more or less close to an intermediate reference line (yellow dashed line in fig. 7). They exhibit different $\varepsilon_{Nd(T)}$ values, ranging from (−2) to near zero or slightly positive values, suggesting derivation from protoliths which include some degree of assimilation of older material. Negative $\varepsilon_{Nd(T)}$ values were also recorded by one sample of the Serra da Bocaina felsic volcanics and two samples of granitoid rocks of the Paso Bravo Province of Paraguay.

The correlation between the groupings defined with the help of Sm-Nd T_{DM} model ages (table 4) suggests that the Sm-Nd systems (fig. 7) were not significantly modified after their formation within the rock protoliths and have always behaved as separated systems. Moreover, the older rock system, with late Archean Sm-Nd T_{DM} model ages, exhibits negative $\varepsilon_{Nd(T)}$ values, while the younger ones, with late Early Proterozoic Sm-Nd T_{DM} model ages, present slightly positive $\varepsilon_{Nd(T)}$ values. This evidence makes unsustainable the hypothesis of a possible derivation from each other. We consider that the resulting alignments showed in figure 7 may have a time significance related to the age of the principal magmatic events that occurred in the area. In this case, the Nd isotopic signatures may indicate that, from the late Archean to the late Paleoproterozoic, there were successive periods of accretion tectonics.

TECTONIC EVOLUTION

Considering the geochronological systematics, a significant improvement has occurred in the geological knowledge of the Rio Apa region. As a consequence, a new reconnaissance map, which is presented in figure 8, has been produced using Lacerda-Filho and others' (2006) map as a basic framework. In addition, this figure includes the observations of the senior author, made during a short trip to the area in 2003, and the observations of A. S. Ruiz from his field work conducted in the region, as well as the information obtained from the reconnaissance geologic map of Wiens (ms, 1986) in Paraguay.

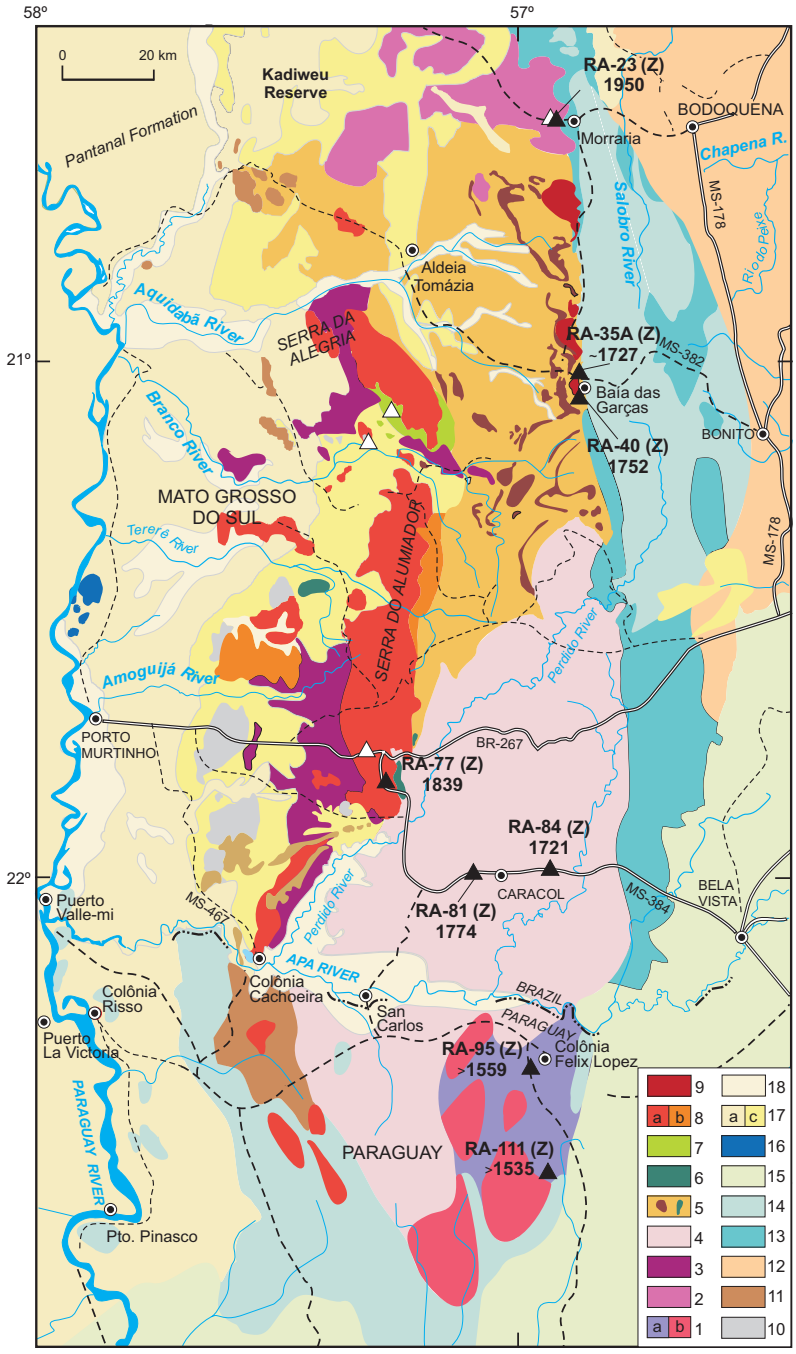

Fig. 8. Geologic outline of the Rio Apa Craton in SW Mato Grosso do Sul (Brazil) and northeastern Paraguay. Adapted from Lacerda Filho and others (2006)—on Brazilian side; adapted from Wiens (ms, 1986), on Paraguayan side. Field observations of UGC and ASR were also taken into consideration. Filled triangles indicate the location of the new U-Pb SHRIMP zircon ages (in bold) and the open triangles indicate the location of the previous U-Pb SHRIMP zircon ages (see fig. 2). Map legend: *Paleoproterozoic units:* 1) Passo Bravo Province (a—banded gneisses; b—migmatites); 2) Morraria banded gneisses; 3) Porto Murtinho banded gneisses; 4) Caracol leucocratic gneisses; 5) Alto Tererê Group (schists, gneisses, granites, amphibo-

TABLE 5

Summary of the Precambrian geologic framework of the Rio Apa Craton. See text and figures 8 and 10 for details

Unit	Main lithologies and exposure areas	Significant radiometric age (Ma)	Geologic correlations and tectonic inferences
Amolar metamorphic domain	Quartzites, sericite-schists and metavolcanics, intruded by granitoid plutons (near Rio Apa River)	-	Strongly folded, low-grade metamorphic supracrustals
Serra da Alegria magmatic suite	Anorthosites, leucogabbros and melagabbros	1791*	Alumiador Batholith
Serra da Bocaina Volcanics	Porphyritic rhyolites, dacites, pyroclastic rocks and volcanic breccias (east of Porto Murtinho)	1794*	Slightly deformed felsic volcanic rocks over the Porto Murtinho basement rocks
Baía das Garças granites	Slightly foliated granitoid rocks near Morraria and Baía das Garças	1754 ± 42**	Granitic rocks intruded into the Alto Tererê Group
Caracol leucocratic gneisses	Foliated, biotite-poor, leucocratic orthogneisses (nearby Caracol and western Paso Bravo province)	1774 ± 26** 1721 ± 25**	Strongly deformed, medium- to high-grade orthogneiss (arc type affinity)
Alto Tererê Group	Garnet-muscovite-biotite schists and minor muscovite-biotite gneisses with quartzite intercalations	-	Medium- to high-grade metasedimentary and metavolcanic rocks and associated basic intrusive rocks
Alumiador granitic batholith	Fine-to-medium grained, pink to gray, isotropic syeno- to monzogranitic rocks (Serra do Alumiador)	1839 ± 33**	Slightly deformed felsic magmatic rocks intruded into the Porto Murtinho basement rocks
Paso Bravo Province	Hornblende-biotite banded gneisses and migmatites intruded by granites (Colonia Felix Lopez, Paraguay)	1846 ± 47***	Paleoproterozoic crystalline basement
Morraria basement	Banded gneisses and migmatites, minor amphibolites	1950 ± 23**	Medium- to high-grade basement rocks (Paleoproterozoic arc)
Porto Murtinho basement	Banded gneisses and migmatites, minor amphibolites	-	Medium- to high-grade basement rocks (Paleoproterozoic arc)

* U-Pb zircon ages as reported by Lacerda-Filho and others (2006). Analytical data not available.
** U-Pb zircon ages; this work (figs. 4, A to F).
*** Rb-Sr isochron age (fig. 6A).

The main changes regarding the tectono-stratigraphic column presented in figure 2, introduced in figure 8 and summarized in table 5, as a consequence of integrated interpretation of the new isotopic data, are the following:

(1) the Rio Apa Complex of Lacerda-Filho and others (2006) can be subdivided into three lithostratigraphic units, as shown by the different U-Pb zircon ages and/or Sm-Nd model ages: Morraria banded gneisses, Porto Murtinho banded gneisses and Caracol leucocatic gneisses. Their main lithologies were described above in the "GEOLOGICAL SETTING" section, when dealing with the Rio Apa Complex.

(2) the Baía das Garças granites, which are intrusive into the Alto Tererê Group in the northeastern part of the region, are distinguished from the Alumiador Suite of Lacerda-Filho and others (2006).

lites); 6) Triunfo complex (gabbroic rocks); 7) Serra da Alegria gabbro-anorthosite suite; 8) Alumiador Batholith (a—granites; b—microgranites); 9) Baía das Garças Granite; 10) Serra da Bocaina Group (rhyolites, dacites, pyroclastic and volcanic breccias); 11) Amolar Domain (schists, quartzites). *Neoproterozoic units* (Paraguay belt): 12) Cuiabá Group; 13) Corumbá Group (Cercadinho Formation); 14) Corumbá and Itapocumi Groups (Bocaina and Tamengo Formations). *Carbonifeous:* 15) Aquidauana Formation; *Triassic:* 16) Fecho dos Morros Alkaline suite. *Pleistocene:* 17) Pantanal Formation; Alluvium (a), Colluvium (c). *Holocene:* 18) Alluvium deposits.

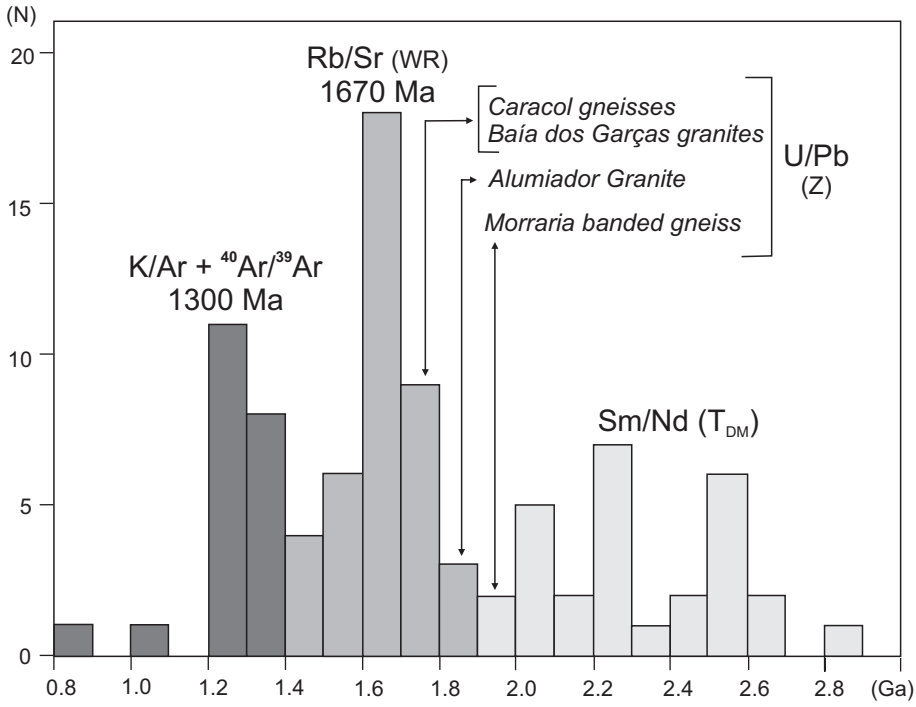

Fig. 9. Histogram of the age determinations obtained on rocks from the Rio Apa Craton. It includes the Sm-Nd T_{DM} model ages, the Rb-Sr whole rock model ages for high $^{87}Rb/^{86}Sr$ ratios, the K-Ar plus ^{39}Ar-^{40}Ar mineral ages, as well as the U/Pb zircon (Z = zircon) ages.

(3) the Paso Bravo Province of Wiens (ms, 1986) is introduced as a distinct lithostratigraphic unit in the Paraguayan portion of the region.

The available radiometric data are significant for determining the timing of relevant episodes within the Rio Apa Craton, and, therefore, for interpreting the regional tectonic evolution. In general, most pre-Neoproterozoic basement rocks seem to be related to a series of magmatic arc complexes, whose material originated from different sources at different times. In effect, the Sm-Nd systematics (table 4, fig. 7) clearly point to variable proportions between juvenile and reworked component in the magmatic rocks, indicating divergent amounts of reworked crustal materials in the original magmas.

Figure 9 is a histogram in which all geochronological data are plotted. The unusual feature is that, despite the reasonably large number of determinations, there is no overlap among the ages obtained by the different dating methods. The Sm-Nd model ages are all older than 1.9 Ga, the calculated Rb-Sr ages are all between 1.4 and 1.9 Ga, and the argon ages are all younger than 1.4 Ga. The Sm-Nd T_{DM} model ages display three peaks, at 2.0, 2.2 and 2.5 Ga. However, only one peak is evident for the Rb-Sr analyses at 1.7 Ga, and the peak that is prominent for the K-Ar and ^{40}Ar-^{39}Ar analyses is at 1.3 Ga.

The position of the U-Pb SHRIMP zircon ages in figure 9 relates to the magmatic crystallization ages of the different units, all of them formed during the Paleoproterozoic. The oldest age, 1950 Ma, was obtained from one granitoid gneiss of the Morraria basement collected in the northern part of the area and is possibly related to the formation of a magmatic arc. The second, 1840 Ma, marks the intrusion of the

Alumiador suite. Finally, the youngest event, dated between 1720 and 1780 Ma, is related to the formation of the Caracol magmatic arc, which is more or less coeval with the granitic intrusions within the Alto Tererê schists in the Baía das Garças area. Two additional and relevant magmatic events, both dated by one sample only at about 1790 Ma, whose position is indicated in figures 2 and 8, are the felsic volcanic rocks of the Serra da Bocaina and the gabbro-anorthositic magmatism of the Serra da Alegria suite.

Regarding the Sm-Nd method, the three peaks observed in figure 9 are related to the isotopic signature of the regional tectonic units, as a response to the nature of the source material and the particular characteristics of the crustal evolution. As discussed in the pertinent section, the Alumiador granites and Serra da Alegria magmatic suite, as well as the Porto Murtinho banded gneisses of the western part of the region, belong to the oldest group of T_{DM} ages (about 2.5-2.6 Ga). The second group (2.2-2.3 Ga) comprises the Caracol leucocratic gneisses, the Serra da Bocaina volcanics, as well as some gneissic and granitic rocks of the Alto Tererê Group and the Paso Bravo Province. The granitic rocks of Baía das Garças, associated with the Alto Tererê metamorphic rocks, belong to the third group (2.0-2.1 Ga).

The Rb-Sr, K-Ar and ^{40}Ar-^{39}Ar methods were applied consistently to the entire region, independently of the character of the analyzed samples. The tectonic interpretation is as follows:

1—At about 1670 Ma, a widespread regional Sr isotopic homogenization episode occurred, possibly related to ductile tectonics in some rocks and to medium- to high-grade pervasive metamorphism in others.

2—At about 1300 Ma, a regional heating event affected the whole region, attaining a temperature of at least 350–400°C, as suggested by the argon blocking temperature in micas.

Considering the distribution of the Sm-Nd model ages, the region can be divided by a boundary into western and eastern domains and, therefore, considered tentatively as two distinct tectonic blocks within the Rio Apa Craton. The western block would encompass the Porto Murtinho banded gneisses of the western basement, the Alumiador and the Serra da Alegria intrusions, the Amolar metasedimentary rocks and the Serra da Bocaina felsic volcanics. The eastern domain would include the Morraria banded gneisses, the Alto Tererê schists, the Baía das Garças granitic rocks, the Caracol leucocratic gneisses and the gneisses, granites and migmatites of the Paso Bravo Province.

Figure 10 is a sketch map that represents this idea, where the two tectonic blocks are displayed side by side, separated by a roughly meridian boundary along the eastern border of the Alumiador batholith. To the north, this boundary deflects to a NW trend along the northern side of the Serra da Alegria. To the south, it follows a NE trend along the Perdido River and deflects to a NNW trend in Paraguay, along the boundary of the Amolar rocks. This inferred limit can be readily seen in the SLAR or satellite images.

We believe that this important discontinuity is a major transcurrent or transpressional fault zone, suturing two different tectonic domains that were juxtaposed at 1680 Ma, when the principal regional deformation affected the entire area, as indicated by the Rb-Sr systematics. The direction of the main compressional tectonic transport, which was responsible for the welding of both terranes, would probably have been from East to West. Moreover, the eastern terrane, which contains rock units formed at a lower crustal level than those of the western block, would probably have been the overriding one. From that time on, the unified Rio Apa block behaved as one tectonically stable cratonic mass.

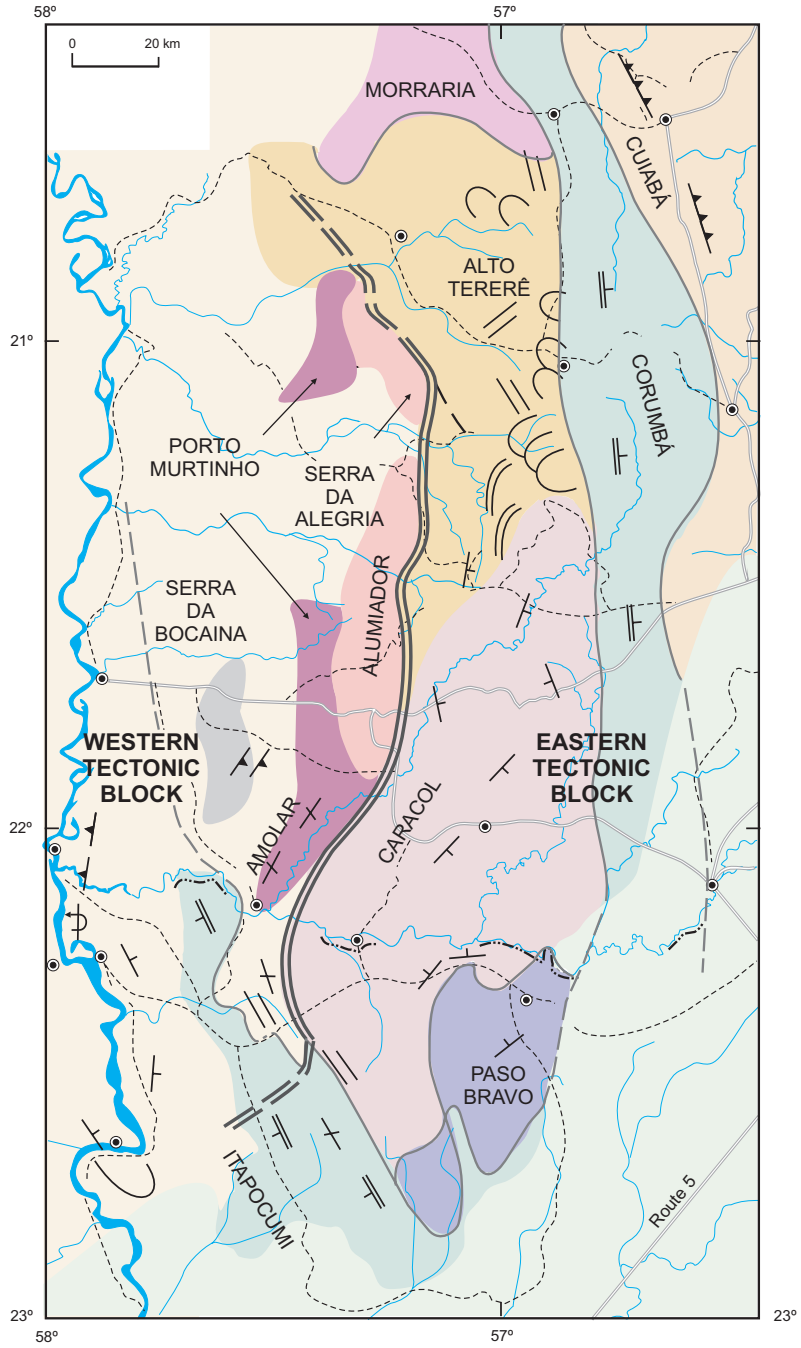

Fig. 10. Tectonic outline of the Rio Apa Craton showing the Western and Eastern tectonic blocks, on the basis of geographical distribution of the Sm-Nd model ages and lithotectonic units. See text for details.

Finally, considering the available geological, petrological, structural and geochronological data, as well the tectonic inferences, some concluding comments, which are summarized in table 5, can be made as follows:

1—The oldest age was obtained from banded gneiss rocks occurring in the northern part of the region, near Morraria. The tectonic significance of these rocks is still obscure, but, tentatively, they may be considered either as an outcrop of an exotic ancient terrain or as a tectonic inlier within the younger Alto Tererê metamorphic rocks. Basement gneisses are found intruded by the Paleoproterozoic Alumiador Suite in the western tectonic domain of the region, near Porto Murtinho. The Amolar metasedimentary rocks, intruded by granitic rocks, also belong to this western block.

2—Within the eastern domain, the Alto Tererê supracrustals were intruded by the late Paleoproterozoic Baía das Garças granites at about 1750 Ma. A similar age is reported by Lacerda-Filho and others (2006) for gneisses interleaved with the supracrustal rocks. Very likely these gneisses, belonging to the Alto Tererê Group, are coeval with the Caracol orthogneisses, occurring to the south, and probably formed in a series of successive magmatic arcs between 1780 and 1720 Ma. As indicated by the Rb-Sr data, all these units were regionally metamorphosed at medium- to high-grade at about 1670 Ma.

3—Approximately 1300 Ma ago, the Rio Apa Craton was affected by widespread regional heating, when the temperature for the entire region exceeded 350°C. Unambiguous tectonic features related to this thermal episode have not yet been described.

4—At the eastern border of the Rio Apa Craton, the Paraguay-Araguaia belt was formed (Almeida, 1967) during the latest Neoproterozoic. Thrust faults related to the tectonic front of the Cuiabá Group are observed, showing a tectonic transport from east-northeast. However, in the basement rocks, only a weak high-level brittle faulting can be attributed to Neoproterozoic tectonics.

5—The eastward low-angle dips of the Corumbá Group and the westward low-angle dips of the coeval Itapocumi Group were produced by high-level gentle folding, forming a structural high corresponding to the outcrops of the Rio Apa Craton. We believe this may be interpreted as a reflection of the Andean mobility related to plate convergence and interaction of relatively small plates, such as Pampia or Arequipa-Antofalla (Ramos, 2008), during the early Paleozoic. The moderate fold and thrust features at Valle-Mi, which were suggested by Campanha and others (2008) to be part of an extensive folded belt, may be alternatively interpreted as an activated aulacogen formed over the Rio Apa Craton.

GEOTECTONIC CORRELATIONS

The Rio Apa Craton, whose regional tectonic evolution has been described on the basis of geologic and geochronologic constraints, correlates well with the SW corner of the Amazonian Craton, where the Mesoproterozoic granitic and gneissic rocks of the Juruena-Rio Negro tectonic province (Tassinari and others, 1996b), with ages between 1600 and 1780 Ma, were affected by tectonic events related to the younger, adjacent Rondonian-San Ignacio province (1560-1300 Ma, according to Bettencourt and others, 2010). A strong metamorphic imprint at 1300 Ma is indicated by U-Pb ages of zircon rims and ^{40}Ar-^{39}Ar dates on country rocks (Teixeira and others, 2006; Cordani and Teixeira, 2007; Santos and others, 2008).

Considering that Amazonia and Laurentia were adjacent in the Neoproterozoic, the relevant question for this time is the tectonic significance of the Tucavaca belt (see fig. 1), as mentioned in the introductory section. The deformation of this belt, such as the observed tectonic dislocation, could be considered as a consequence of contempo-

rary extensional tectonic episodes, resulting from the separation at the terminal Precambrian of these large continents. Nevertheless, it is considered that Amazonia and Laurentia merged along a Grenville-Sunsás collisional belt at approximately 1000 to 1100 Ma, and, therefore, it is likely that the extensional deformation observed in the Tucavaca aulacogen was a tectonic reactivation, affecting a weakened crust at the site of this Mesoproterozoic collisional suture.

In pre-Neoproterozoic times, the situation seemed to be quite different, depending on the very complex interaction between Laurentia and Amazonia during the entire Proterozoic. The interplay between them may have started much earlier, seeing that plate convergence is observed in both cratonic nuclei, marked by successive and more or less synchronous accretionary and/or collisional episodes since the Paleoproterozoic. In the Appalachian margin of Laurentia, the Labradorian, Pinwarian, Elsonian, Elzevirian, Shawinigan, Ottawan and Rigolet orogenic pulses were witnesses of the continued convergent efforts, which lasted almost 1000 Ma and whose tectonic polarity was always directed to the West, towards the stable ancient craton (Gower and Krogh, 2002; Tollo and others, 2004; Bartholomew and others, 2010). Only the last three tectonic pulses, Shawinigan, Ottawan and Rigolet, are considered to belong to the "Grenville orogeny." On the other hand, in the southwestern margin of Amazonia, during the same time-span, the Ventuari-Tapajós, Rio Negro-Juruena, Rondonian-San Ignacio and Sunsás-Aguapeí provinces were formed by successive partly accretionary and partly collisional pulses, where direction was always from NE to SW and tectonic polarity was directed towards the ancient core located to the north and northeast (Cordani and Teixeira, 2007; Teixeira and others, 2010).

Sadowski and Bettencourt (1996), in their article on the Laurentia-Amazonia collision, proposed two complete Wilson cycles, with formation and disappearance of oceanic domains, culminating in the Sunsás orogeny in the latest Mesoproterozoic, at approximately 1000 to 1100 Ma, when Rodinia was forming. Moreover, as a precursor of the Sunsás orogeny, the Rondonian-San Ignacio orogeny is another major crustal event, active roughly between 1560 and 1300 Ma and affecting a large area along the Brazilian-Bolivian border (Bettencourt and others, 2010). At least part of this orogeny was synchronous with the Pinwarian and Elzevirian orogenies in Canada. In conclusion, Laurentia and Amazonia, after a complex and long lasting interplay, became welded at the end of the Mesoproterozoic as part of Rodinia and remained together until their separation at about 570 Ma, when the Iapetus Ocean was formed.

The repeated cycles of convergence and separation between Laurentia and Amazonia during the Mesoproterozoic produced a complex arrangement of allochthonous blocks of different sizes, which were trapped during the collisions of the main continental masses (fig. 11). They may have originated as disrupted parts of either Laurentia or Amazonia, or newly formed accretionary terranes of an intervening ocean (Ramos, 1988 and 2009). One of the largest was the Paraguá block, which is partly accretionary and partly a reworked crustal fragment. This block was welded to the Rio Negro-Juruena province during the final accretionary events that characterize the Rondonian-San Ignacio composite orogeny (Bettencourt and others, 2010). Later, it behaved as a stable cratonic landmass for the Sunsás belt (Litherland and others, 1989; Boger and others, 2005; Teixeira and others, 2010). Remnants of other terranes, largely covered by Mesozoic to Cenozoic sedimentary basins or by Andean volcanic and sedimentary rocks, whose outcrops are dispersed over a large area, making correlations difficult, are the Arequipa, Antofalla, Pampia, (Ramos, 2008 and 2009), and include the Rio Apa Craton.

The Arequipa and Antofalla terranes are key features for the Laurentia-Amazonia ties. They may have been generated during the separation of Laurentia from Gondwana at about 570 Ma (Li and others, 2008), and could have returned later to South

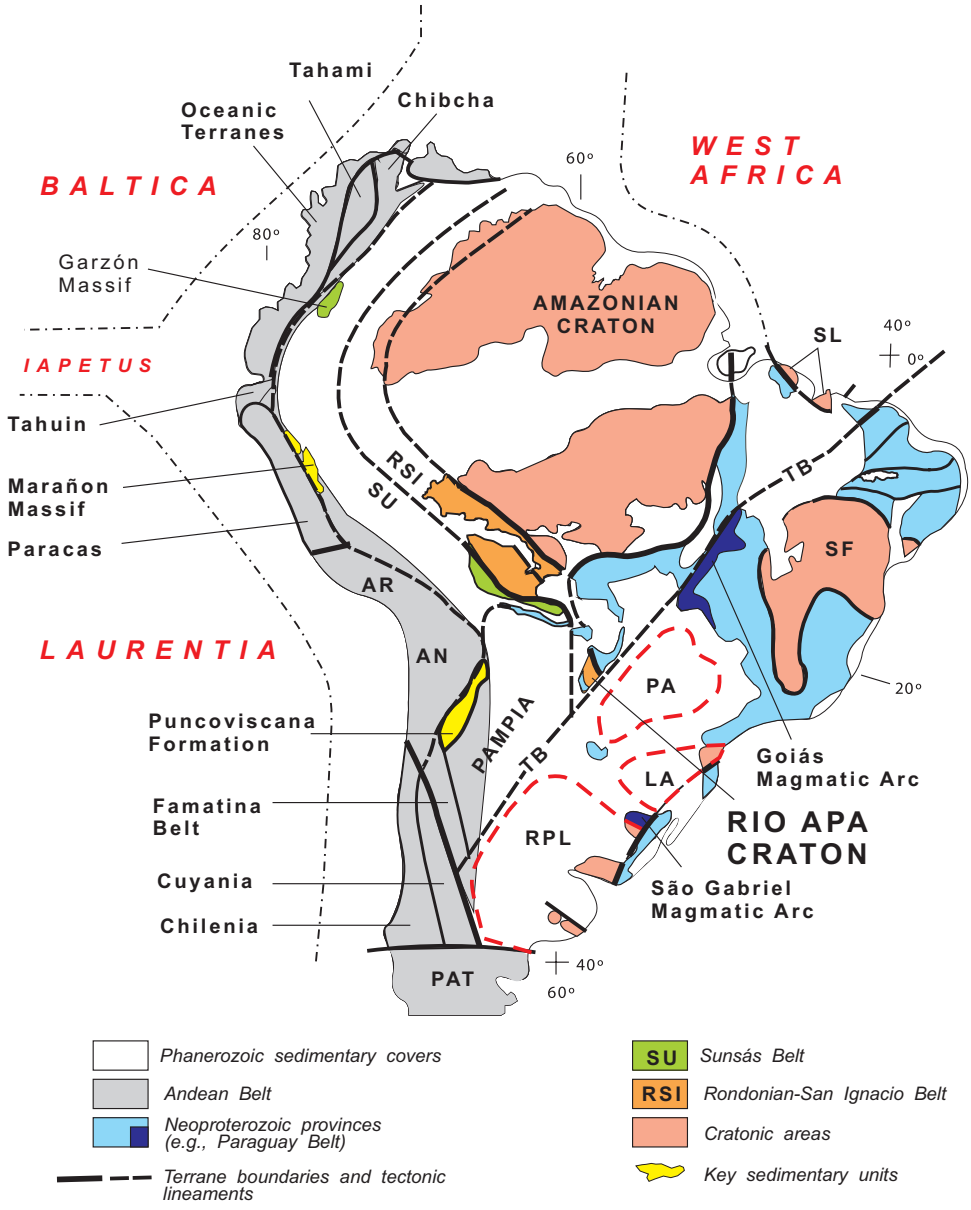

Fig. 11. Geotectonic sketch map of South America with the tentative outline of allochthonous blocks of different sizes, possibly trapped during the various collisions of Laurentia and Gondwana. The possible distribution of the Mesoproterozoic Rondonian-San Ignacio (RSI) and Sunsás (SU) tectonic provinces, overlain by Phanerozoic sedimentary cover is also suggested. Most nomenclature of key tectonic elements is included in the figure. TB = *Transbrasiliano Lineament.* Cratonic areas: *Amazonian Craton;* SL = *São Luiz,* SF = *São Francisco,* PA = *Paranapanema,* LA = *Luiz Alves,* RPL = *Rio de La Plata.* Allochthonous terranes: AR = *Arequipa,* AN = *Antofalla,* PAT = *Patagonia.*

America, as allochthonous units, during the early Paleozoic. Paleoproterozoic to Paleozoic ages were obtained from their rocks, indicating a very complex history (Ramos, 2008 and 2009). Pampia is largely unknown, since it is almost entirely overlain

by Phanerozoic sediments of the Chaco Basin. The early Paleozoic sediments of the Puncoviscana Formation in northern Argentina (shown in fig. 11) contain a great deal of detrital zircons with Grenvillian-type ages, most probably from sources derived from Pampia (Zimmerman, 2005; Ramos, 2009). This suggests that this terrane may include accretionary systems of Grenvillian-Sunsás age, which were formed during the assembly of Rodinia. Moreover, Adams and others (2008) have shown that detrital zircon ages of 1700 to 1800 Ma also occur and could easily be related to the Rio Apa Craton.

Possible correlations of the Rio Apa Craton with these allochthonous terranes and also with Amazonia should consider the complex tectonic evolution of the former, where basement rocks of Paleoproterozoic age were affected by strong heating in the Mesoproterozoic. In this respect, as mentioned above, the best possible correlation is with the Rio Negro-Juruena tectonic province, at the SW portion of the Amazonian Craton. However, an alternative correlation can be made with the Paraguá block (Bolivia), where the main tectonic pattern was formed during the Rondonian-San Ignacio orogeny, but where important Paleoproterozoic basement inliers were identified. These are the Lomas-Manechi medium- to high-grade gneisses, which were described by Litherland and others (1989) and recently dated by U-Pb SHRIMP zircon (Boger and others, 2005; Santos and others, 2008), yielding ages of 1660 to 1700 Ma, but also inherited ages of 1820 Ma. A correlation of the Rio Apa Craton with the Arequipa block can also be attempted due to the presence of the older rocks of the latter (Loewy and others, 2004; Ramos, 2008). However, a correlation with either Antofalla or Pampia is more difficult, because these terranes seem to be made essentially of younger rocks linked to the Sunsás orogeny.

A different kind of correlation can be made when it is noticed that large regions of Amazonia, especially in the northern part, were affected by widespread heating at about 1200 to 1300 Ma. This Mesoproterozoic event, related to intra-plate heating in several large areas and accompanied by isotopic rejuvenation of micas, was named the K'Mudku tectono-thermal episode by Barron (1969) in Guyana and the Nickerie metamorphic episode by Priem and others (1971) in Suriname and Colombia. This matter was thoroughly reviewed by Cordani and others (2010) for the entire Amazonian Craton, but the geodynamic significance of the pervasive heating needs to be investigated in further detail. However, as pointed out by Cordani and others (2010), extended areas affected by the K'Mudku/Nickerie event are located at the western limit of the Guiana Shield, adjacent to the Llanos Basin, foreland for the Andean mountain belt. Priem and others (1982), obtained in eastern Colombia a few U-Pb zircon ages between 1560 and 1780 Ma, which allow correlation with the Rio Negro-Juruena province.

In figure 11, a possible continuation of the Rondonian-San Ignacio province under the Solimões and Acre sedimentary basins is traced. In this case, a correlation with the Rio Apa Craton is possible because similar K-Ar and ^{40}Ar-^{39}Ar radiometric ages at approximately 1300 Ma were obtained on minerals from the older "basement" rocks. The physical significance of these apparent ages is the time of cooling below a critical temperature (about 350-400°C), which may be interpreted in two ways, either as a response to some localized thermal event, or to the normal cooling associated with regional uplift after cratonization. For both the Rio Apa and Paraguá tectonic blocks, the 1300 Ma apparent ages of micas should be considered as related to crustal exhumation and cratonization of the Rondonian-San Ignacio orogeny. Following Cordani and others (2010), we assume that the similar regional cooling ages obtained in eastern Colombia by Priem and others (1971) indicate the extension of the Rondonian-San Ignacio Province, making up large parts of the Llanos Basin of Colombia and Venezuela (fig. 11).

In Bolivia, the Sunsás collisional belt outcrops at the south-westernmost extremity of the Amazonian Craton, and is disposed parallel to and overprinting the Rondonian-San Ignacio province. Figure 11 shows its possible continuation, below the Phanerozoic basins, towards the north-west and bending further to the north, as proposed initially by Kroonenberg (1982) and more recently by many others, including Ramos (2008 and 2009) and Cordani and others (2010). Good evidence for this is the Grenvillian/Sunsás age of detrital zircons in many Paleozoic sedimentary units, such as the Puncoviscana Formation in Argentina and the Paleozoic units adjacent to the Marañon massif in Peru, both indicated in figure 11 (Cardona and others, 2009). Moreover, the Garzón Massif in Colombia, also indicated in figure 11, yielded K-Ar ages between 1000 to 1100 Ma (Jimenez and others, 2006), showing that it was not affected by the Andean tectono-thermal episodes. We consider that the Marañon and Garzón massifs are the best evidence for the position of the western limits of the autochthonous or para-autochthonous basement to the Andean belt.

Figure 11 includes, as suggested by the present authors and discussed in the text, the proposed outline of the main geotectonic units at the time of agglutination of West Gondwana. The tentative outline of the Amazonian Craton, specifically its Mesoproterozoic tectonic provinces, considering the Paraguá block as the main constituent of the Rondonian-San Ignacio Province, is traced in figure 11. Moreover, as discussed above, the possible western and northern boundaries of this province, as well as those of the adjacent Sunsás Province, are also shown is this figure. The Paracas, Tahuín, Arequipa, Antofalla and Pampia allochthonous terranes, which were welded to Amazonia in Precambrian times, are also indicated in figure 11. Pampia has a special geotectonic significance because it seems to be a direct continuation of the Sunsas collisional belt. Since many detrital zircons from Pampia show igneous derivation, most probably from a magmatic arc setting, it is possible that much of this terrane is made up of Grenvillian age accretionary material. Also, the early Paleozoic Famatina belt, at the western margin of Pampia, contains detrital zircons with Grenvillian ages. Moreover, younger allochthonous terranes, which were incorporated in South America during the Phanerozoic (Ramos, 2009), are also shown in figure 11. Many of them include either basement inliers with Grenvillian ages, like the Chibcha and Tahami terranes of Colombia (Cordani and others, 2005b), or sedimentary rocks with detrital zircon, like the Cuyania or Chilenia terranes (Ramos, 2009).

The Transbrasiliano lineament, which cuts the continent from NE to SW and is the major suture along which a large ocean disappeared (Pimentel and others, 1997) during the process of agglutination of Gondwana, is the most significant Neoproterozoic tectonic feature of South America. It includes the major Neoproterozoic intra-oceanic Goiás magmatic arc, which was witness of the great ocean that separated the large supercontinent including Laurentia, Amazonia, Baltica and West Africa, from the large São Francisco-Congo continental mass, plus smaller cratonic fragments, such as the Rio de La Plata, Luiz Alves and Paranapanema. All Precambrian crustal nuclei plotted in figure 11 at the north-western side of the Transbrasiliano lineament show affinities with the Amazonian Craton, to which the Mesoproterozoic tectonic units of the Rondonian-San Ignacio and Sunsás belts are attached. In this manner, rocks formed between approximately 1500 and 1000 Ma are predominant in the SW corner of Amazonia and are also very common in the basement of the Andean belt. On the other hand, at the south-eastern side of the Transbrasiliano lineament, the São Francisco-Congo Craton and the smaller cratonic nuclei mentioned above (large parts of which are hidden below the sediments of the Paraná Basin), usually do not contain Mesoproterozoic domains and were not affected by tectonic events of that age. As a consequence, both sides of the Transbrasiliano lineament show marked differences in their tectonic evolution. In the case of the Rio Apa Craton, there is a strong correlation

with the north-western tectonic units, in which Mesoproterozoic elements are common. On the contrary, it shows no affinity at all with the south-eastern tectonic units.

We consider, as a final remark, that the Amazonian Craton, to which the Rio Apa cratonic block was attached, is one of the building blocks of Rodinia. However, the significant contrast between the tectonic evolution of the continental crust at the opposite sides of the Transbrasiliano lineament, together with the possibility of the existence of a very large oceanic domain prior to the Neoproterozoic suture, makes a possible correlation of the Rio Apa basement rocks with the tectonic units occurring to the south-east of the lineament very difficult. This led Kröner and Cordani (2003) and Cordani and others (2003) to suggest that the cratonic fragments occurring to the southeast of the lineament may never had been part of that supercontinent.

ACKNOWLEDGMENTS

This research received support from the Brazilian National Research Council (CNPq) through grants 302851/2004 to UGC and grants 471585/2007 and 302917/2009-8 to WT. Fruitful discussions with Fernando Wiens and Joffre Lacerda-Filho are acknowledged. In addition, the authors received useful comments from Benjamin Bley de Brito-Neves, Jorge Silva Bettencourt, Ginaldo Campanha and Maria Helena Bezerra Maia de Hollanda at the USP. UGC is most grateful to Paulo Cesar Boggiani and Narciso Cubas, who accompanied him during field work in 2003. Finally, the authors greatly acknowledge the referees R. Pankhurst and V. Ramos, as well as Guest Editor S. Wilde for their careful criticism and helpful suggestions made to the early version of this manuscript.

Appendix 1

SHRIMP U-Pb data

Sample	U (ppm)	Th (ppm)	$^{232}Th/^{238}U$ (ppm)	$^{206}Pb_{Rad}$ (ppm)	$\%^{206}Pb_c$	204corr $^{206}Pb^*/^{238}U$ Age (Ma)	1 σ error	204corr $^{207}Pb^*/^{206}Pb^*$ Age (Ma)	1 σ error	% Disc	$^{207}Pb^*/^{206}Pb^*$	% err	$^{207}Pb^*/^{235}U$	% err	$^{206}Pb^*/^{238}U$	% err	err. corr.
MORRARIA BANDED GNEISSES																	
RA-23																	
1	248	214	0.89	76	0.42	1963	25	1936	22	-1	0.1186	1.2	5.82	1.9	0.3559	1.5	0.767
3	459	315	0.71	129	0.11	1829	23	1920	15	5			5.32	1.7	0.3280	1.4	0.854
5	383	350	0.94	96	0.09	1654	20	1932	16	14			4.78	1.7	0.2926	1.4	0.851
6	197	165	0.87	60	0.11	1950	26	1968	19	1	0.1208	1.1	5.88	1.9	0.3532	1.5	0.819
9	228	148	0.67	68	0.00	1920	25	1955	17	2	0.1199	1.0	5.73	1.8	0.3469	1.5	0.837
8	359	205	0.59	88	0.55	1610	20	1895	22	15			4.54	1.9	0.2837	1.4	0.754
ALUMIADOR GRANITIC SUITE																	
RA-77																	
1.1	190	147	0.80	52.	0.23	1784	42	1879	27	5	0.1150	1.5	5.05	3.1	0.3188	2.7	0.874
2.1	132	114	0.89	40	14.67	1673	48			8	0.1108	13.6	4.53	14.0	0.2964	3.3	0.234
3.1	77	84	1.12	19	0.13	1626	43	1889	40	14			4.57	3.7	0.2870	3.0	0.802
4.1	666	700	1.09	154	1.60	1516	35	1787	34	15			3.99	3.2	0.2651	2.6	0.811
5.1	156	168	1.11	44	1.16	1816	45	1796	60	-1	0.1098	3.3	4.93	4.4	0.3255	2.9	0.654
6.1	266	503	1.95	69	2.02	1665	39	1787	61	7	0.1093	3.4	4.44	4.3	0.2946	2.7	0.621
7.1	773	680	0.91	207.	0.15	1749	39	1820	13	4	0.1112	0.7	4.78	2.6	0.3116	2.5	0.961
8.1	133	124	0.96	37	1.35	1764	44	1854	55	5	0.1134	3.0	4.92	4.1	0.3147	2.8	0.681
9.1	98	82	0.87	15.	5.28	1020	30			44			2.61	10.0	0.1714	3.2	0.320
BAIA DAS GARÇAS GRANITES																	
RA-35																	
1	254	257	1.05	65	0.32	1671	22			4	0.1067	1.4	4.35	2.1	0.2960	1.5	0.712
2	446	345	0.80	83	2.38	1232	21	1499	150	18	0.0936	7.9	2.72	8.1	0.2107	1.9	0.231
3.1	331	453	1.41	78	0.87	1549	20	1639	35	6	0.1008	1.9	3.78	2.4	0.2716	1.4	0.611
3.2	263	282	1.11	63	0.54	1569	21			10	0.1067	1.6	4.05	2.2	0.2755	1.5	0.673
5	553	264	0.49	103	0.50	1259	16			18	0.0951	1.4	2.83	2.0	0.2157	1.4	0.707
6	2048	1197	0.60	141	16.61	417	7	1242	240	66	0.0818	12.3	0.75	12.4	0.0667	1.7	0.138
7	357	584	1.69	58	3.55	1086	18	1662	72	35	0.1021	3.9	2.58	4.3	0.1836	1.8	0.420
9	246	206	0.86	63	0.42	1673	22	1727	29	3	0.1057	1.6	4.32	2.2	0.2963	1.5	0.695
RA-40																	
2.1	319	229	0.74	55	0.96	1162	28	1710	43	32	0.1048	2.3	2.85	3.6	0.1976	2.7	0.751
3.1	117	105	0.93	31	0.00	1740	44	1734	35	0	0.1062	1.9	4.53	3.4	0.3098	2.9	0.835
4.1	210	109	0.54	54	0.24	1698	40	1765	30	4	0.1079	1.7	4.49	3.2	0.3014	2.7	0.853

Appendix 1

(continued)

Sample	U (ppm)	Th (ppm)	$^{232}Th/^{238}U$ (ppm)	$^{206}Pb_{Rad}$ (ppm)	$\%^{206}Pb_c$	204corr $^{206}Pb^*/^{238}U$ Age (Ma)	1 σ error	204corr $^{207}Pb^*/^{206}Pb^*$ Age (Ma)	1 σ error	% Disc	$^{207}Pb^*/^{206}Pb^*$	% err	$^{207}Pb^*/^{235}U$	% err	$^{206}Pb^*/^{238}U$	% err	err. corr.
BAIA DAS GARÇAS GRANITES																	
RA-40																	
5.1	137	126	0.94	22	2.11	1090	29	1519	106	28	0.0946	5.6	2.40	6.3	0.1842	2.9	0.455
6.1	302	238	0.82	74	2.15	1582	37	1796	50	12	0.1098	2.8	4.21	3.8	0.2781	2.6	0.692
7.1	264	223	0.87	58	0.16	1464	35	1734	25	16	0.1062	1.4	3.73	3.0	0.2550	2.7	0.889
8.1	254	141	0.57	38	2.00	1012	26	1734	74	42	0.1061	4.1	2.49	4.9	0.1700	2.7	0.559
10.1	146	148	1.04	25	1.42	1134	30	1617	83	30	0.0996	4.5	2.64	5.3	0.1923	2.8	0.535
CARACOL LEUCOCRATIC GNEISSES																	
RA-81																	
1.1	2071	2408	1.20	168	3.47	562	14	1378	57	59	0.0878	3.0	1.10	3.9	0.0911	2.5	0.652
2.1	297	283	0.98	72	0.08	1601	37	1768	20	9	0.1081	1.1	4.20	2.8	0.2819	2.6	0.920
2.1	503	1151	2.37	88	0.40	1191	28	1649	23	28	0.1013	1.3	2.83	2.9	0.2029	2.6	0.897
5.1	523	616	1.22	63	0.46	846	20	1598	29	47	0.0986	1.5	1.91	3.0	0.1403	2.6	0.856
6.1	664	206	0.32	51	0.15	548	14	539	44	-2	0.0582	2.0	0.71	3.2	0.0887	2.6	0.790
7.1	887	1467	1.71	73	1.24	585	14	1512	41	61	0.0942	2.2	1.23	3.4	0.0951	2.6	0.767
7.2	388	379	1.01	82	0.06	1420	33	1752	19	19	0.1072	1.1	3.64	2.8	0.2464	2.6	0.925
8.1	679	1431	2.18	49	3.99	501	13	1450	93	65	0.0911	4.9	1.02	5.5	0.0808	2.6	0.474
9.1	151	165	1.13	35	1.00	1508	38	1640	63	8	0.1008	3.4	3.66	4.4	0.2636	2.8	0.637
10.1	824	1380	1.73	79	0.79	679	17	1451	34	53	0.0912	1.8	1.40	3.1	0.1110	2.6	0.821
11.1	239	240	1.04	59	0.10	1620	45	1773	25	9	0.1084	1.4	4.27	3.4	0.2857	3.1	0.916
RA-84																	
1	121	85	0.72	32	0.20	1722	26	1724	29	0	0.1056	1.6	4.46	2.3	0.3062	1.7	0.736
2	106	90	0.88	30	0.40	1811	28	1713	34	-6	0.1049	1.8	4.69	2.6	0.3244	1.8	0.689
3	101	75	0.77	27	0.73	1741	27	1714	49	-2	0.1050	2.7	4.49	3.2	0.3101	1.8	0.555
4	119	95	0.83	33	0.26	1794	27	1757	37	-2	0.1075	2.0	4.75	2.6	0.3209	1.7	0.651
5	198	237	1.24	53	0.46	1734	23	1667	29	-4	0.1024	1.6	4.36	2.2	0.3087	1.5	0.692
6	151	144	0.98	41	0.12	1751	25	1757	27	0	0.1075	1.5	4.63	2.2	0.3121	1.6	0.734
6	92	71	0.80	25	0.87	1749	28	1709	58	-2	0.1047	3.1	4.50	3.6	0.3116	1.8	0.498

APPENDIX 1

(continued)

Sample	U (ppm)	Th (ppm)	$^{232}Th/^{238}U$ (ppm)	$^{206}Pb_{Rad}$ (ppm)	$\%^{206}Pb_c$	204corr $^{206}Pb^*/^{238}U$ Age (Ma)	1 σ error	204corr $^{207}Pb^*/^{206}Pb^*$ Age (Ma)	1 σ error	% Disc	$^{207}Pb^*/^{206}Pb^*$	% err	$^{207}Pb^*/^{235}U$	% err	$^{206}Pb^*/^{238}U$	% err	err. corr.
PASO BRAVO PROVINCE																	
RA-95																	
1.1	2298	144	0.06	247	3.20	736	18		-	30			1.24	4.1	0.1209	2.5	0.623
1.2	2269	231	0.11	252	1.33	773	19	1371	42	44			1.54	3.4	0.1274	2.6	0.757
2.1	2337	1099	0.49	356	0.49	1046	24		-	31			2.29	2.6	0.1762	2.5	0.950
3.1	2250	5227	2.40	149	6.37	450	11	1426	96	68			0.90	5.7	0.0723	2.6	0.461
3.2	1209	1264	1.08	151	1.92	858	21	1535	48	44			1.87	3.6	0.1423	2.6	0.710
4.1	1117	756	0.70	146	4.52	874	21.	1410	73	38			1.79	4.6	0.1452	2.6	0.558
5.1	311	128	0.42	51	1.61	1116	27	1397	61	20	0.0887	3.2	2.31	4.1	0.1889	2.6	0.642
5.2	1427	1529	1.11	199	14.11	841	21	1472	177	43			1.77	9.7	0.1394	2.7	0.279
6.1	219	17	0.08	38	1.85	1177	30	1323	102	11	0.0853	5.3	2.36	6.0	0.2004	2.8	0.462
7.1	195	28	0.15	32	0.49	1138	29	1418	50	20	0.0897	2.6	2.39	3.9	0.1931	2.8	0.732
8.1	420	74	0.18	73	0.56	1183	28	1355	41	13	0.0867	2.1	2.41	3.4	0.2013	2.6	0.777
8.3	1418	821	0.60	149	6.81	694	17	1204	118	42			1.26	6.5	0.1136	2.6	0.399
9.1	2224	246	0.11	430	0.17	1307	30		-	21			3.14	2.6	0.2248	2.5	0.964
RA-111																	
2.1	1845	645	0.36	271	5.21	967	23	1419	68	32	0.0897	3.6	2.00	4.4	0.1619	2.5	0.580
3.1	1859	298	0.17	269	1.04	992	23	1525	22	35	0.0948	1.1	2.18	2.8	0.1664	2.5	0.910
4.1	1492	253	0.18	286.	0.30	1295	30	1544	16	16			2.94	2.7	0.2224	2.5	0.950
5.1	905	235	0.27	174	0.94	1287	30			24			3.16	2.8	0.2210	2.5	0.900
6.1	1222	337	0.29	211	0.59	1175	27			28			2.78	2.7	0.2000	2.5	0.926
7.1	2378	1018	0.44	219	10.88	587	15	1491	127	61			1.22	7.2	0.0953	2.6	0.362
8.1	2107	1009	0.50	233	1.72	769	18	1462	31	47			1.60	3.0	0.1268	2.5	0.838
9.1	2760	1057	0.40	407	0.54	1017	24			20			1.96	2.6	0.1708	2.5	0.960
10.1	1619	667	0.43	251	4.37	1027	24	1559	55	34	0.0966	2.9	2.30	3.9	0.1726	2.5	0.653
11.1	1363	617	0.47	216	7.14	1020	25	1516	106	33	0.0944	5.6	2.23	6.2	0.1715	2.6	0.423

Pb* corrected using ^{204}Pb.

Appendix 2

Ar-Ar data

Sample	Lab#	Laser (W)	40/39	38/39	37/39	36/39	40*/39	%Rad	Ar40 (moles)	Age (Ma)	± (Ma)
RAPA-88C	1916-01A	0.30	371.351	0.022	5.199	0.009	370.334	99.4	6.37E-14	1360.4	4.9
amphibole	1916-01B	0.60	346.633	0.022	3.387	0.004	346.372	99.7	7.03E-14	1297.5	5.7
	1916-01C	0.90	337.234	0.025	10.059	0.021	333.921	98.4	7.60E-15	1263.9	15.2
	1916-01D	1.20	357.807	0.139	65.942	0.179	324.011	86.6	1.44E-15	1236.7	107.3
	1916-01E	3.18	335.901	0.104	58.145	0.148	308.362	88.3	1.70E-15	1193.0	50.1
RAPA-93A	1917-01A	0.30	1542.389	-0.000	0.000	0.118	1507.26	97.7	6.56E-15	3101.9	154.6
amphibole	1917-01B	0.60	724.266	0.014	14.514	0.023	725.387	99.2	4.38E-14	2101.1	12.0
	1917-01C	0.89	398.808	0.022	57.005	0.023	411.698	99.3	4.74E-15	1464.0	47.1
	1917-01D	1.29	456.958	0.058	115.086	0.100	471.995	95.4	1.60E-15	1605.2	68.9
	1917-01E	3.17	419.983	0.028	52.270	0.028	430.572	99.0	4.95E-15	1509.4	27.5
	1917-02A	0.35	498.169	0.018	0.000	0.037	486.983	97.8	1.87E-14	1638.7	18.0
	1917-02B	0.50	523.405	0.013	15.557	0.015	525.416	99.4	3.41E-14	1721.7	8.9
	1917-02C	0.60	329.102	0.028	15.382	0.027	325.372	97.9	7.40E-15	1240.5	15.2
	1917-02D	0.89	376.876	0.011	0.925	-0.004	378.551	100.4	6.58E-15	1381.4	25.9
	1917-02E	1.39	356.410	0.018	18.688	0.019	356.390	98.8	4.10E-15	1324.0	28.0
	1917-02F	2.99	357.978	0.011	10.322	0.010	358.196	99.4	1.26E-14	1328.8	12.9
RAPA-112	1918-01A	0.15	315.620	0.013	0.002	0.007	313.465	99.3	9.83E-14	1207.4	4.2
biotite	1918-01B	0.25	345.098	0.012	0.000	0.001	344.708	99.9	1.29E-13	1293.0	3.3
	1918-01C	0.32	342.925	0.012	0.000	0.003	341.911	99.7	5.87E-14	1285.5	10.0
	1918-01D	0.45	343.227	0.012	0.000	0.000	343.086	100.0	5.73E-14	1288.7	5.3
	1918-01E	0.55	338.878	0.015	0.059	0.006	337.115	99.5	3.18E-14	1272.6	7.7
	1918-01F	0.65	352.0280	0.012	0.000	0.000	351.958	100.0	8.68E-15	1312.3	18.2
	1918-01G	0.80	351.334	0.005	0.000	-0.013	355.238	101.1	6.47E-15	1321.0	18.5
	1918-01H	1.09	340.558	0.017	0.000	0.009	337.899	99.2	1.07E-14	1274.7	14.9
	1918-01I	2.97	313.468	0.016	0.000	0.037	302.448	96.5	4.32E-15	1176.2	23.0
	1918-02A	0.08	19.592	2.147	346.031	2.664	-960.881	-	-2.66E-18	0.0	-
	1918-02B	0.15	278.261	0.014	0.055	0.007	276.137	99.2	5.75E-14	1099.4	4.2
	1918-02C	0.20	337.043	0.013	0.069	0.001	336.605	99.9	8.81E-14	1271.2	3.8
	1918-02D	0.25	343.921	0.013	0.241	0.001	343.687	99.9	5.93E-14	1290.3	4.4
	1918-02E	0.35	350.312	0.011	0.000	-0.000	350.374	100.0	6.93E-14	1308.1	5.2
	1918-02F	0.50	343.176	0.011	0.000	0.000	343.088	100.0	5.56E-14	1288.7	5.8
	1918-02G	0.70	343.024	0.008	0.000	-0.004	344.349	100.4	4.43E-14	1292.1	6.0
	1918-02H	3.19	336.237	0.011	1.277	0.001	336.047	99.9	2.54E-14	1269.7	8.8
	1918-03A	0.08	253.196	0.011	0.000	0.012	249.437	98.5	4.19E-15	1018.0	19.3
	1918-03B	0.15	326.072	0.015	0.311	0.007	323.822	99.3	5.01E-14	1236.2	4.9
	1918-03C	0.20	345.071	0.012	0.000	0.001	344.635	99.9	5.60E-14	1292.8	5.8
	1918-03D	0.25	346.275	0.010	0.000	-0.000	346.288	100.0	3.54E-14	1297.2	16.1
	1918-03E	0.35	348.095	0.016	0.192	0.008	345.778	99.3	4.87E-14	1295.9	6.2
	1918-03F	0.50	336.398	0.011	0.000	0.002	335.698	99.8	4.03E-14	1268.7	6.6
	1918-03G	0.70	327.879	0.020	0.193	0.009	324.995	99.1	2.36E-14	1239.5	9.9
	1918-03H	3.19	319.341	0.020	0.582	0.012	315.786	98.8	1.55E-14	1213.9	12.1
RAPA-114	1919-01A	0.10	155.273	0.034	1.054	0.059	137.861	88.7	4.98E-15	631.4	11.6
biotite	1919-01B	0.20	335.770	0.014	0.000	0.003	334.689	99.7	1.45E-13	1266.0	4.0
	1919-01C	0.30	346.821	0.014	0.000	0.002	346.192	99.8	1.94E-13	1297.0	3.0
	1919-01D	0.45	353.098	0.014	0.033	0.002	352.340	99.8	2.34E-13	1313.3	3.0
	1919-01E	0.55	348.824	0.013	0.003	0.001	348.414	99.9	1.23E-13	1302.9	3.3
	1919-01F	0.70	350.996	0.014	0.035	0.001	350.418	99.8	1.14E-13	1308.3	4.2
	1919-01G	0.90	349.103	0.013	0.000	0.000	348.837	99.9	8.36E-14	1304.0	9.0
	1919-01H	1.39	349.372	0.021	0.759	0.010	346.469	99.1	2.28E-14	1297.7	7.8
	1919-01I	2.34	350.393	0.036	0.000	0.009	347.587	99.2	1.70E-15	1300.7	55.4
	1919-02A	0.12	258.706	0.010	0.040	0.026	250.932	97.0	1.97E-14	1022.6	7.2
	1919-02B	0.20	339.126	0.014	0.015	0.002	338.290	99.8	1.45E-13	1275.8	3.3
	1919-02C	0.25	349.820	0.011	0.000	0.000	349.743	100.0	1.34E-13	1306.5	3.9
	1919-02D	0.35	346.970	0.014	0.000	0.001	346.398	99.8	1.73E-13	1297.5	3.9
	1919-02E	0.40	348.613	0.015	0.034	0.004	347.182	99.6	8.30E-14	1299.6	4.2
	1919-02F	0.50	347.367	0.015	0.000	0.001	346.934	99.9	1.40E-13	1299.0	3.5
	1919-02G	0.70	344.858	0.013	0.000	-0.001	345.198	100.1	1.57E-13	1294.3	3.7
	1919-02H	0.90	342.775	0.011	0.000	-0.000	342.922	100.0	7.26E-14	1288.2	4.9
	1919-02I	1.39	340.303	0.002	0.012	-0.000	340.444	100.0	1.40E-14	1281.6	15.6
	1919-02J	3.19	351.906	0.006	0.000	-0.012	355.487	101.0	8.63E-15	1321.7	24.5
	1919-03A	0.12	-1.919	0.493	135.614	0.558	-171.940	-	-2.92E-19	1333.9	2201.0
	1919-03B	0.20	324.803	0.016	0.000	0.010	321.849	99.1	2.10E-13	1230.7	4.4
	1919-03C	0.25	343.502	0.015	0.000	0.001	342.981	99.8	1.19E-13	1288.4	4.6
	1919-03D	0.35	349.702	0.013	0.016	0.003	348.701	99.7	2.55E-13	1303.7	3.3
	1919-03E	0.40	347.952	0.014	0.000	0.001	347.366	99.8	2.06E-13	1300.1	4.6
	1919-03F	0.50	350.019	0.015	0.065	0.002	349.162	99.8	1.65E-13	1304.9	3.8

Appendix 2

(continued)

Sample	Lab#	Laser (W)	40/39	38/39	37/39	36/39	40*/39	%Rad	Ar40 (moles)	Age (Ma)	± (Ma)
RAPA-114	1919-03G	0.70	348.132	0.014	0.055	0.002	347.553	99.8	2.31E-13	1300.6	4.9
biotite	1919-03H	0.90	338.801	0.014	0.051	0.001	338.369	99.9	9.37E-14	1276.0	4.1
	1919-03I	3.19	340.345	0.014	0.002	0.000	340.052	99.9	1.65E-13	1280.5	3.4
RAPA-83	1920-01A	0.10	73.826	0.004	0.000	0.001	73.494	99.6	4.48E-15	363.7	4.1
biotite	1920-01B	0.20	258.484	0.010	0.000	0.001	258.174	99.9	1.06E-13	1045.0	3.3
	1920-01C	0.30	287.326	0.012	0.000	0.000	287.193	100.0	2.72E-13	1132.0	2.4
	1920-01D	0.45	288.605	0.012	0.019	0.000	288.397	99.9	3.21E-13	1135.6	2.5
	1920-01E	0.55	285.548	0.010	0.000	-0.001	285.911	100.1	1.12E-13	1128.3	3.8
	1920-01F	0.80	284.515	0.012	0.025	-0.000	284.652	100.0	1.20E-13	1124.6	4.5
	1920-01G	1.39	263.083	0.009	0.000	-0.003	264.183	100.4	1.89E-14	1063.4	7.1
	1920-01H	2.55	231.742	0.010	0.000	-0.001	232.114	100.2	2.74E-14	963.1	5.5
	1920-02A	0.12	191.843	0.045	0.000	0.145	148.899	77.6	2.48E-14	673.5	5.3
	1920-02B	0.22	262.552	0.016	0.000	0.030	253.543	96.6	1.46E-13	1030.7	4.2
	1920-02C	0.30	269.554	0.013	0.000	0.010	266.475	98.9	1.20E-13	1070.3	3.4
	1920-02D	0.35	270.545	0.012	0.069	0.008	268.195	99.1	6.54E-14	1075.5	7.9
	1920-02E	0.40	272.765	0.018	0.020	0.006	270.811	99.3	4.87E-14	1083.4	4.8
	1920-02F	0.45	272.826	0.015	0.203	0.004	271.563	99.5	3.82E-14	1085.7	5.2
	1920-02G	0.55	271.265	0.015	0.000	0.005	269.752	99.4	3.43E-14	1080.2	4.4
	1920-02H	0.80	273.628	0.012	0.089	0.005	271.997	99.4	3.49E-14	1087.0	6.1
	1920-02I	1.49	265.160	0.017	0.000	0.009	262.361	98.9	2.15E-14	1057.8	5.8
	1920-02J	3.18	288.617	-0.017	0.000	-0.026	296.564	102.8	3.32E-15	1159.3	23.4
	1920-03A	0.12	236.555	0.010	0.000	0.005	234.972	99.3	2.92E-14	972.3	4.9
	1920-03B	0.23	274.493	0.011	0.000	0.001	274.126	99.9	1.53E-13	1093.4	3.0
	1920-03C	0.30	278.626	0.012	0.000	0.001	278.177	99.8	9.15E-14	1105.4	3.4
	1920-03D	0.40	278.041	0.013	0.118	0.002	277.303	99.7	7.63E-14	1102.8	4.5
	1920-03E	0.50	277.027	0.011	0.123	-0.000	277.071	100.0	5.17E-14	1102.2	4.8
	1920-03F	0.60	273.740	0.011	0.204	-0.000	274.046	100.1	3.55E-14	1093.1	6.4
	1920-03G	0.80	273.706	0.013	0.126	-0.000	274.012	100.1	2.90E-14	1093.0	6.5
	1920-03H	1.59	272.879	0.007	0.000	-0.004	274.239	100.5	2.76E-14	1093.7	5.7
	1920-03I	3.19	242.078	0.097	9.191	0.068	223.807	91.9	1.43E-15	936.2	42.0
RAPA-76	1921-01A	0.20	330.100	0.012	0.000	0.004	328.654	99.6	1.58E-13	1249.5	2.8
biotite	1921-01B	0.35	350.381	0.012	0.118	0.000	350.254	100.0	2.95E-13	1307.8	2.8
	1921-01C	0.50	348.120	0.011	0.000	0.000	347.878	99.9	2.31E-13	1301.5	2.8
	1921-01D	0.80	346.132	0.010	0.067	0.000	346.010	100.0	1.68E-13	1296.5	3.5
	1921-01E	3.17	341.452	0.011	2.527	0.003	341.160	99.7	3.22E-14	1283.5	8.7
	1921-02A	0.20	343.532	0.012	0.509	0.003	342.656	99.7	1.22E-13	1287.5	3.8
	1921-02B	0.30	349.189	0.012	1.079	0.001	348.955	99.9	8.94E-14	1304.4	4.0
	1921-02C	0.50	347.160	0.014	1.088	0.002	346.874	99.8	7.85E-14	1298.8	4.5
	1921-02D	2.99	347.670	0.020	2.827	0.005	347.060	99.6	2.11E-14	1299.3	8.6
RAPA-52	1922-01A	0.20	144.733	0.333	8.208	0.084	121.223	83.3	3.13E-16	565.9	85.6
muscovite	1922-01B	0.35	382.348	-0.030	0.000	-0.063	401.174	104.9	1.48E-15	1438.2	68.9
	1922-01C	0.50	368.145	0.059	0.000	0.047	354.230	96.2	4.15E-15	1318.3	33.0
	1922-01D	0.89	346.070	0.012	0.553	0.002	345.563	99.8	2.55E-13	1295.3	2.9
	1922-01E	3.18	328.069	0.031	17.441	-0.011	336.656	101.4	5.22E-15	1271.3	30.9
	1922-02A	0.50	344.272	0.013	0.000	0.003	343.379	99.7	1.43E-13	1289.5	5.3
	1922-02B	0.65	344.012	0.016	1.635	0.003	343.596	99.8	2.81E-14	1290.0	7.3
	1922-02C	0.85	349.416	0.019	0.000	-0.036	360.230	103.1	4.67E-15	1334.1	25.7
	1922-02D	2.99	337.674	0.018	0.000	-0.002	338.497	100.2	2.05E-14	1276.3	8.0
RAPA-62F	1923-01A	0.20	264.019	0.016	0.276	0.016	259.113	98.1	9.02E-14	1047.9	3.2
biotite	1923-01B	0.35	302.805	0.014	0.000	0.011	299.314	98.8	7.58E-14	1167.2	3.2
	1923-01C	0.50	301.502	0.015	0.000	0.006	299.541	99.3	3.42E-14	1167.8	5.7
	1923-01D	0.80	308.550	0.015	0.334	0.006	306.723	99.4	2.60E-14	1188.3	6.6
	1923-01E	3.17	312.970	0.009	2.933	0.001	313.511	100.0	1.47E-14	1207.5	14.0
	1923-02A	0.15	315.642	0.012	0.261	0.004	314.425	99.6	6.22E-14	1210.1	3.6
	1923-02B	0.30	345.665	0.012	0.002	0.001	345.125	99.8	1.70E-13	1294.1	2.9
	1923-02C	0.50	345.719	0.012	0.000	0.000	345.512	99.9	9.37E-14	1295.2	3.4
	1923-02D	3.19	347.132	0.003	0.000	-0.003	348.243	100.3	2.11E-14	1302.5	9.2
RAPA-18B	1926-01A	0.20	115.124	0.017	0.000	0.010	112.129	97.4	1.65E-14	509.8	3.2
muscovite	1926-01B	0.35	114.113	0.011	0.000	0.000	114.033	99.9	1.57E-13	517.3	1.2
	1926-01C	0.50	114.278	0.009	0.000	-0.002	114.961	100.6	4.71E-15	521.0	7.1
	1926-01D	0.89	115.614	0.016	0.000	-0.000	115.669	100.0	1.00E-14	523.8	4.4
	1926-01E	3.18	110.459	0.020	1.045	0.007	108.411	98.1	4.80E-15	495.0	5.8
	1926-02A	0.20	115.549	0.014	1.073	0.009	112.989	97.7	1.81E-14	513.2	2.8
	1926-02B	0.27	114.704	0.011	0.010	0.000	114.555	99.9	1.20E-13	519.4	1.3
	1926-02C	0.40	113.046	0.011	0.057	0.000	112.834	99.8	1.01E-13	512.6	1.1
	1926-02D	0.90	112.875	0.006	0.000	0.000	112.692	99.8	8.20E-15	512.0	4.3
	1926-02E	2.99	115.196	0.010	0.000	0.000	114.998	99.8	2.08E-14	521.1	2.6

Appendix 2

(continued)

Sample	Lab#	Laser (W)	40/39	38/39	37/39	36/39	40*/39	%Rad	Ar40 (moles)	Age (Ma)	± (Ma)
RAPA-22	1927-01A	0.20	318.017	0.029	0.000	0.029	309.200	97.2	5.26E-15	1158.4	21.5
muscovite	1927-01B	0.35	359.348	0.012	0.000	-0.000	359.386	100.0	2.92E-13	1292.1	2.6
	1927-01C	0.55	355.394	0.011	0.074	0.000	355.334	100.0	5.64E-13	1281.7	2.4
	1927-01D	0.90	356.176	0.010	0.000	0.000	355.904	99.9	1.40E-13	1283.1	3.6
	1927-01E	3.18	354.345	0.012	0.410	0.001	354.122	99.9	1.25E-13	1278.5	3.3
	1927-02A	0.25	354.425	0.009	0.000	0.001	354.066	99.9	1.19E-13	1278.4	3.4
	1927-02B	0.35	356.977	0.012	0.337	0.000	356.978	100.0	3.41E-13	1285.9	3.0
	1927-02C	0.50	349.687	0.013	0.000	-0.000	349.798	100.0	1.10E-13	1267.3	11.8
	1927-02D	0.89	358.089	0.012	0.000	0.001	357.695	99.9	5.83E-14	1287.7	5.2
	1927-02E	2.99	357.752	0.014	1.490	0.003	357.224	99.8	3.23E-14	1286.5	6.8
RAPA-23	1929-01A	0.20	320.240	0.012	0.000	0.005	318.550	99.5	1.03E-13	1184.1	3.0
biotite	1929-01B	0.35	345.813	0.013	0.067	0.002	345.125	99.8	1.66E-13	1255.1	3.2
	1929-01C	0.50	350.955	0.011	0.000	-0.000	351.003	100.0	8.51E-14	1270.4	5.4
	1929-01D	0.80	351.596	0.010	0.000	-0.003	352.515	100.3	3.50E-14	1274.4	6.5
	1929-01E	3.18	348.385	0.001	0.000	-0.004	349.715	100.4	2.58E-14	1267.1	8.0
	1929-02A	0.15	324.916	0.013	0.000	0.003	323.889	99.7	8.38E-14	1198.6	4.6
	1929-02B	0.25	342.329	0.012	0.000	0.000	342.315	100.0	3.00E-13	1247.7	14.0
	1929-02C	0.35	354.577	0.011	0.000	-0.000	354.684	100.0	2.01E-13	1280.0	4.6
	1929-02D	0.50	350.335	0.010	0.000	0.000	350.157	99.9	2.45E-13	1268.2	3.3
	1929-02E	2.99	351.226	0.010	0.000	0.000	351.207	100.0	2.42E-13	1271.0	2.6
RAPA-32	1930-01A	0.25	362.139	0.011	0.000	0.001	361.763	99.9	2.26E-13	1298.2	2.6
muscovite	1930-01B	0.40	363.017	0.010	0.000	-0.001	363.402	100.1	1.13E-13	1302.4	4.0
	1930-01C	0.60	368.261	-0.003	4.946	0.013	365.760	99.0	1.12E-14	1308.4	18.6
	1930-01D	0.85	378.291	-0.028	0.000	-0.051	393.460	104.0	7.03E-15	1377.5	22.9
	1930-01E	2.76	365.590	0.009	0.000	0.000	365.578	100.0	4.87E-14	1307.9	6.4
	1930-02A	0.12	310.103	0.009	16.611	0.038	303.362	96.8	4.62E-15	1142.2	26.7
	1930-02B	0.25	364.276	0.013	0.000	0.002	363.675	99.8	1.41E-13	1303.1	3.2
	1930-02C	0.40	362.016	0.013	0.021	0.000	361.825	99.9	3.20E-13	1298.3	2.6
	1930-02D	0.89	358.324	0.013	2.142	0.000	358.760	100.0	7.08E-14	1290.5	4.9
	1930-02E	2.99	362.834	0.015	0.000	0.000	362.679	100.0	3.34E-14	1300.5	8.6
RAPA-37A	1932-01A	0.15	347.037	0.013	0.740	0.001	346.887	99.9	1.01E-13	1259.7	3.7
biotite	1932-01B	0.25	365.244	0.010	0.000	-0.001	365.549	100.1	1.38E-13	1307.8	2.8
	1932-01C	0.35	367.689	0.011	0.000	-0.000	367.734	100.0	1.05E-13	1313.4	4.0
	1932-01D	0.55	360.871	0.007	0.778	0.001	360.532	99.9	6.82E-14	1295.0	4.1
	1932-01E	2.76	351.257	0.025	6.848	0.009	350.698	99.4	1.45E-14	1269.6	10.9
	1932-02A	0.15	326.768	0.015	0.997	0.005	325.336	99.5	4.12E-14	1202.5	6.0
	1932-02B	0.25	360.357	0.013	0.574	0.001	359.970	99.9	1.71E-13	1293.6	3.4
	1932-02C	0.35	365.117	0.012	0.000	0.000	364.967	100.0	2.40E-13	1306.4	3.2
	1932-02D	0.50	366.548	0.012	0.000	0.000	366.380	100.0	2.21E-13	1310.0	3.0
	1932-02E	2.99	367.989	0.011	0.000	0.000	367.891	100.0	3.82E-13	1313.8	2.7
RAPA-33	1933-01A	0.25	364.123	0.013	0.000	0.001	363.738	99.9	1.25E-13	1303.2	4.1
muscovite	1933-01B	0.40	364.791	0.013	0.000	0.000	364.674	100.0	7.59E-14	1305.6	4.7
	1933-01C	0.60	359.835	0.012	1.534	-0.001	360.626	100.1	3.93E-14	1295.3	7.1
	1933-01D	0.80	359.554	0.018	3.207	0.005	359.001	99.6	3.29E-14	1291.1	6.7
	1933-01E	2.34	360.382	0.015	0.466	0.001	360.106	99.9	4.50E-14	1293.9	7.2
	1933-02A	0.15	320.764	0.024	0.000	0.009	318.102	99.2	1.75E-15	1182.9	59.5
	1933-02B	0.35	363.191	0.013	0.000	0.005	361.694	99.6	1.05E-13	1298.0	3.9
	1933-02C	0.80	361.685	0.015	0.017	0.006	359.907	99.5	4.61E-14	1293.4	7.1
	1933-02D	2.99	364.027	0.011	0.000	-0.001	364.364	100.1	3.76E-14	1304.8	7.0
RAPA-38	1935-01A	0.15	359.288	0.010	0.000	-0.001	359.810	100.1	1.13E-13	1293.2	3.6
biotite	1935-01B	0.25	366.371	0.010	0.000	0.000	366.238	100.0	1.04E-13	1309.6	3.9
	1935-01C	0.35	361.606	0.007	0.000	-0.001	362.043	100.1	6.97E-14	1298.9	6.0
	1935-01D	0.55	367.667	0.002	0.000	-0.004	369.002	100.4	2.68E-14	1316.6	10.6
	1935-01E	2.34	380.361	0.020	0.000	0.004	378.936	99.6	8.45E-15	1341.6	23.2
	1935-02A	0.01	10.641	1.764	871.051	2.155	-1319.760	-	3.14E-18	0.0	-
	1935-02B	0.20	349.511	0.015	2.969	0.005	348.900	99.6	7.43E-14	1265.0	4.7
	1935-02C	0.35	362.326	0.012	0.324	0.000	362.299	100.0	2.63E-13	1299.5	2.6
	1935-02D	2.99	365.692	0.011	0.427	0.000	365.680	100.0	4.63E-13	1308.2	2.6
RAPA-45	1936-01A	0.25	484.852	0.017	0.000	0.520	331.091	68.3	1.73E-15	1217.9	98.7
muscovite	1936-01B	0.40	354.179	0.011	0.000	0.000	353.914	99.9	3.92E-13	1278.0	2.3
	1936-01C	0.60	352.407	0.018	2.290	0.007	350.771	99.4	2.69E-14	1269.8	7.7
	1936-01D	0.85	323.566	0.063	14.225	0.051	312.473	95.7	3.89E-15	1167.4	30.2
	1936-01E	2.55	346.776	0.028	7.898	0.018	343.720	98.6	1.17E-14	1251.4	12.9
	1936-02A	0.32	204.536	0.372	0.000	0.700	-2.394	-1.2	2.30E-16	-12.6	523.9
	1936-02B	0.40	185.182	0.505	238.790	0.323	128.322	58.3	2.36E-16	572.8	299.3
	1936-02C	0.60	382.478	0.049	0.000	0.026	374.763	98.0	3.59E-15	1331.1	48.2
	1936-02D	2.99	358.591	0.012	0.142	0.001	358.274	99.9	4.86E-13	1289.2	3.5

References

Adams, C. J., Miller, H., Toselli, A. J., and Griffin, W., 2008, The Puncoviscana Formation of northwest Argentina: U-Pb geochronology of detrital zircons and Rb-Sr metamorphic ages and their bearing on its stratigraphic age, sediment provenance and tectonic setting: Neues Jahrbuch fur Geologie und Pälaontologie—Abhandlungen, v. 247, p. 341–352, doi: 10.1127/0077-7749/2008/0247-0341.

Almeida, F. F. M. de, 1965, Geologia da Serra da Bodoquena (Mato Grosso): Boletim DNPM, Divisão de Geologia e Mineralogia, v. 219, p. 1–137.

——— 1967, Origem e Evolução da Plataforma Brasileira: Boletim DNPM, Divisão de Geologia e Mineralogia, v. 241, p. 1–36.

Alvarenga, C. J. S., and Saes, G. S., 1992, Estratigrafia e sedimentologia do Proterozóico Médio e Superior da região sudeste do Craton Amazônico: Revista Brasileira de Geociências, v. 22, n. 4, p. 493–499.

Alvarenga, C. J. S., Moura, C. A. V., Gorayeb, P. S. S., and Abreu, F. A. M., 2000, Paraguay and Araguaia Belts, *in* Cordani, U. G., Milani, E. J., Thomas-Filho, A., and Campos, D. A., editors, Tectonic Evolution of South America: Rio de Janeiro, 31° International Geological Congress, p. 183–193.

Amaral, G., Cordani, U. G., Kawashita, K., and Reynolds, J. H., 1966, Potassium-Argon dates of basaltic rocks from Southern Brazil: Geochimica et Cosmochimica Acta, v. 30, p. 159–189, doi: 10.1016/0016-7037(66)90105-0.

Araújo, H. J. T., Santos Neto, A., Trindade, C. A. H., Pinto, J. C. A., Montalvão, R. M. G., Dourado, T. D. C., Palmeira, R. C. B., and Tassinari, C. C. G., 1982, Folha SF.21—Campo Grande: geologia, geomorfologia, pedologia, vegetação e uso potencial da terra, *in* Levantamento de Recursos Naturais: Rio de Janeiro, DNPM, Projeto RadamBrasil, v. 28, 416 p.

Ávila-Salinas, W., 1992, El magmatismo Cámbrico-Ordovícico em Bolívia, *in* Gutierrez Marco, J. C., Saavedra, J., and Rábano, I., editors, Paleozoico Inferior de Ibero-America: Extremadura, Universidad de Extremadura, p. 241–253.

Barron, C. N., 1969, Notes on the stratigraphy of Guyana: Geological Survey of British Guiana, v. 6, n. 2, p. 1–28.

Bartholomew, M. J., and Hatcher, R. D., Jr., 2010, The Grenville orogenic cycle of southern Laurentia: Unraveling sutures, rifts, and shear zones as potential piercing points for Amazonia: Journal of South American Earth Sciences, v. 29, p. 4–20, doi: 10.1016/j.jsames.2009.08.007.

Bettencourt, J. S., Leite, W. B., Jr., Ruiz, A. S., Matos-Salinas, G. R., Payolla, B. L., and Tosdal, R. M., 2010, The Rondonian-San Ignacio province in the SW Amazonian Craton: an overview: Journal of South American Earth Sciences, v. 29, p. 28–46, doi: 10.1016/j.jsames.2009.08.006.

Boger, S. D., Raetz, M., Giles, D., Etchart, E., and Fanning, C. M., 2005, U-Pb age data from the Sunsas region of eastern Bolivia, evidence for the allochthonous origin of the Paragua Block: Precambrian Research, v. 139, p. 121–146, doi: 10.1016/j.precamres.2005.05.010.

Boggiani, P. C., and Alvarenga, C. J. S., 2004, A faixa Paraguai, *in* Mantesso-Neto,V., Bartorelli, A., Carneiro, C. D. R., and Brito-Neves, B. B., organizers, Geologia do continente sul-americano: evolução da obra de Fernando Flávio Marques de Almeida: São Paulo, Beca, Brazil, v. 7, p. 113–120.

Boggiani, P. C., Fairchild, T. R., and Coimbra, A. M., 1993, O Grupo Corumbá (Neoproterozóico—Cambriano) na região central da Serra da Bodoquena (Faixa Paraguai), Mato Grosso do Sul: Revista Brasileira de Geociências, v. 23, n. 3, p. 301–305.

Campanha, G. A. C., Boggiani, P. C., Warren, L., Grohmann, C. H., and Caceres, A. A., 2008, Possibilidade de uma nova faixa móvel brasiliana no norte do Paraguai: Anais 44° Congresso Brasileiro de Geologia, p. 33.

Cardona, A., Cordani, U. G., Ruiz, J., Valencia, V. A., Armstrong, R., Chew, D., Nutman, A. P., and Sanchez, A. W., 2009, U-Pb Zircon Geochronology and Nd Isotopic Signatures of the Pre-Mesozoic Metamorphic Basement of the Eastern Peruvian Andes: Growth and Provenance of a Late Neoproterozoic to Carboniferous Accretionary Orogen on the Northwest Margin of Gondwana: The Journal of Geology, v. 117, p. 285–305, doi: 10.1086/597472.

Cordani, U. G., and Teixeira, W., 2007, Proterozoic accretionary belts in the Amazonian Craton, *in* Hatcher, R. D., Jr., Carlson, M. P., McBride, J. H., and Martínez-Catalan, J. R., editors, 4-D Framework of Continental Crust: Boulder, Colorado, Geological Society of America Memoirs 200, p. 297–320, doi: 10.1130/2007.1200(14).

Cordani, U. G., D'Agrella-Filho, M. S., Trindade, R., and Brito-Neves, B. B., 2003, Tearing up Rodinia: The Neoproterozoic palaeogeography of South American cratonic fragments: Terra Nova, v. 15, p. 350–359, doi: 10.1046/j.1365-3121.2003.00506.x.

Cordani, U. G., Tassinari, C. C. G., and Rolim, D. R., 2005a, The basement of the Rio Apa Craton in Mato Grosso do Sul (Brazil) and northern Paraguay: a geochronological correlation with the tectonic provinces of the south-western Amazonian Craton: Mendoza, Proceedings of the 12th Gondwana International Gondwana Symposium Abstracts, p. 112.

Cordani, U. G., Cardona, A., Jimenez, D. M., Liu, D., and Nutman, A. P., 2005b, Geochronology of Proterozoic basement inliers in the Colombian Andes: tectonic history of remnants of a fragmented Grenville Belt, *in* Vaughan, A. P. M., Leat, P. T., and Pankhurst, R. J. editors, Terrane Processes at the Margins of Gondwana: Geological Society, London, Special Publication, n. 246, p. 329–346, doi: 10.1144/GSL.SP.2005.246.01.13.

Cordani, U. G., Tassinari, C. C. G., Teixeira, W., and Coutinho, J. M. V., 2008a, U-Pb SHRIMP zircon ages for the Rio Apa Cratonic Fragment in Mato Grosso do Sul (Brazil) and northern Paraguay: tectonic implications: San Carlos de Bariloche, Argentina, VI South American Symposium on Isotope Geology, Book of Abstracts, p. 1–8.

——— 2008b, The basement of the Rio Apa Craton in Mato Grosso do Sul (Brazil) and northern Paraguay: Tectonic implications and correlations: Oslo, Norway, 5–14 August 2008, 33rd International Geological Congress, AMS-07 Crustal evolution of the cratonic nuclei of South America, Oslo, CD-ROM, Abstract.

Cordani, U. G., Teixeira, W., D'Agrella-Filho, M. S., and Trindade, R. I., 2009, The position of the Amazonian Craton in supercontinents: Gondwana Research, v. 15, p. 396–407, doi: 10.1016/j.gr.2008.12.005.

Cordani, U. G., Fraga, L. M., Reis, N., Tassinari, C. C. G., and Brito-Neves, B. B., 2010, On the origin and tectonic significance of the intra-plate events of Grenvillian-type age in South America: A discussion: Journal of South American Earth Sciences, v. 29, p. 143–149, doi: 10.1016/j.jsames.2009.07.002.

Corrêa, J. A., Neto, C., Correia-Filho, F. C. L., Scislewski, G., Cavallon, L. A., Cerqueira, N. L. S., and Nogueira, V. L., 1976, Projeto Bodoquena: Goiânia, CPRM, v. 8, 110 p. (Relatório final).

Dell'Arco, J. O., Silva, R. H., Tarapanoft, I., Freire, F. A., Pereira, L. G. M., Sousa, S. L., Luz, D. S., Palmeira, R. C. B., and Tassinari, C. C. G., 1982, Folha SE.21—Corumbá e parte da Folha SE.20: geologia, geomorfologia, pedologia, vegetação e uso potencial da terra, *in* BRASIL, Levantamento de Recursos Naturais: Rio de Janeiro, Departamento Nacional da Produção Mineral, Projeto RadamBrasil, v. 27, p. 25–160.

Delgado, I. M., Souza, J. D., Silva, L. C., Silveira-Filho, N. C., Santos, R. A., Pedreira, A. J., Guimarães, J. T., Angelim, L. A. A., Vasconcelos, A. M., Gomes, I. P., Lacerda-Filho, J. V., Valente, C. R., Perrotta, M. M., and Heineck, C. A., 2003, Província Tocantins, *in* Bizzi, L. A., Schobbenhaus, C., Vidotti, R. M., and Gonçalves, J. H., editors, Geologia, Tectônica e Recursos Minerais do Brasil: Rio de Janeiro, CPRM, p. 281–292.

DePaolo, D. J., 1981, A neodymium and strontium isotopic study of the Mesozoic calc-alkaline granitic batholiths of the Sierra Nevada and Peninsular Ranges, California: Journal of Geophysical Research, v. 86, n. B11, p. 10470–10488, doi: 10.1029/JB086iB11p10470.

Godoi, H. O., organizer, 1999, Folha SF.21-X-A—Estado do Mato Grosso do Sul: Aquidauana, *in* Programa Levantamentos Geológicos Básicos do Brasil (PLGB): Brasília, CPRM, 72 p.

Godoi, H. O., Martins, E. G., and Mello, J. C. R., 1999, Folha SE. 21-Y-D—Corumbá, Folha SF.21-V-B—Aldeia Tomázia, Folha SF.21-V-D—Porto Murtinho, escala 1:250.000 *in* Programa de Levantamentos Geológicos Básicos do Brasil (PLGB): Brasília, CPRM.

Godoy, A. M., Manzano, J. C., Araújo, L. M. B. de, and Silva, J. A. da, 2009, Contexto geológico-estrutural do Maciço Rio Apa, sul do Cráton Amazônico-MS: São Pedro, SBG, Anais do Simpósio de Geologia do Sudeste, Abstract, 11/Simpósio de Geologia de Minas Gerais, 15, p. 20.

Gower, C. F., and Krogh, T. E., 2002, A U-Pb geochronological review of the Proterozoic history of the eastern Grenville Province: Canadian Journal Earth Sciences, v. 39, p. 795–829, doi: 10.1139/e01-090.

Jimenez, D. M., Juliani, C., and Cordani, U. G., 2006, P-T-t conditions of high-grade metamorphic rocks of the Garzón Massif, Andean basement, SE Colombia: Journal of South American Earth Sciences, v. 21, p. 322–336, doi: 10.1016/j.jsames.2006.07.001.

Kröner, A., and Cordani, U. G., 2003, African, southern Indian and South American cratons were not part of the Rodinia supercontinent: evidence from field relationships and geochronology: Tectonophysics, v. 375, p. 325–352, doi: 10.1016/S0040-1951(03)00344-5.

Kroonenberg, S. B., 1982, A Grenvillian Granulite Belt in the Colombian Andes and its Relation to the Guiana Shield: Geologie en Mijnbouw, v. 61, p. 325–333.

Lacerda-Filho, J. V., Brito, R. S. C de, Silva, M. G., Oliveira, C. C. de, Moreton, L. C., Martins, E. G., Lopes, R. C., Lima, T. M., Larizatti, J. H., and Valente, C. R., 2006, Geologia e Recursos Minerais do Estado de Mato Grosso do Sul, Programa Integração, Atualização e Difusão de Dados da Geologia do Brasil: Convênio CPRM/SEPROTUR/MS, Campo Grande, 121, escala 1;1.000.000.

Li, Z. X., Bogdanova, S. V., Collins, A. S., Davidson, A., De Waele, B., Ernst, R. E., Fitzsimons, I. C. W., Fuck, R. A., Gladkochub, D. P., Jacobs, J., Karlstrom, K. E., Lu, S., Natapov, L. M., Pease, V., Pisarewsky, S. A., Thrane, K., and Vernikovsky, V., 2008, Assembly, configuration, and break-up history of Rodinia: A synthesis: Precambrian Research, v. 160, p. 179–210, doi: 10.1016/j.precamres.2007.04.021.

Litherland, M., Annels, R. N., Darbyshire, D. P. F., Fletcher, C. J. N., Hawkins, M. P., Klinck, B. A., Mitchell, W. I., O'Connor, E. A., Pitfield, P. E. J., Power, G., and Webb, B. C., 1989, The Proterozoic of Eastern Bolivia and its relationship to the Andean Mobile Belt: Precambrian Research, v. 43, p. 157–174, doi: 10.1016/0301-9268(89)90054-5.

Loewy, S. L., Connelly, J. N., and Dalziel, I. W. D., 2004, An orphaned basement block: the Arequipa-Antofalla basement of the central Andean margin of South America: Geological Society of America Bulletin, v. 116, p. 171–87, doi: 10.1130/B25226.1.

Ludwig, K. R., 2003, Isoplot 3.00: a geochronological toolkit for Microsoft Excel® (revised version): Berkeley Geochronological Center, Special Publication, v. 4, 70 p.

Pimentel, M. M., Whitehouse, M. J., Viana, M. das G., Fuck, R. A., and Machado, N., 1997, The Mara Rosa arc in the Tocantins Province: further evidence for Neoproterozoic crustal accretion in central Brazil: Precambrian Research, v. 81, p. 299–310, doi: 10.1016/S0301-9268(96)00039-3.

Priem, H. N. A., Boelrijk, N. A. I. M., Hebeda, E. H., Verdurmen, E. A. Th., and Verschure, R. H., 1971, Isotopic ages of the Trans-Amazonian acidic magmatism and the Nickerie Metamorphic Episode in the Precambrian Basement of Suriname, South America: Geological Society of America Bulletin, v. 82, p. 1667–1680, doi: 10.1130/0016-7606(1971)82[1667:IAOTTA]2.0.CO;2.

Priem, H. N. A., Andriessen, P. A. M., Boelrijk, N. A. I. M., Hebeda, E. H., Huguett, A., Verdurmen, E. A. Th, and Verschure, R. H., 1982, Geochronology of the Precambrian in the Amazonas Region of southeast Colombia (western Guiana Shield): Geologie en Mijnbouw, v. 61, p. 229–242.

Ramos, V. A., 1988, Late Proterozoic—Early Paleozoic of South America: a collisional history: Episodes, v. 11, p. 168–174.

——— 2008, The basement of the Central Andes: the Arequipa and related terranes: Annual Review of Earth and Planetary Sciences, v. 36, p. 289–324, doi: 10.1146/annurev.earth.36.031207.124304.

——— 2009, Anatomy and global context of the Andes: Main geologic features and the Andean orogenic cycle, *in* Kay, S. M., Ramos, V. A., and Dickinson, W. R., editors, Backbone of the Americas: Shallow Subduction, Plateau Uplift, and Ridge and Terrane Collision: Geological Society of America Memoir 204, p. 31–65, doi: 10.1130/2009.1204(02).

Ruiz, A. S., Simões, L. S. A., and Brito-Neves, B. B., 2005, Maciço Rio Apa: extremo meridional do Cráton Amazônico, *in* Boletim de Resumos Expandidos 10 Simpósio Nacional de Estudos Tectônicos—SNET: Curitiba, Sociedade Brasileira de Geologia, p. 301–304.

Sadowski, G. R., and Bettencourt, J. S., 1996, Mesoproterozoic tectonic correlations between eastern Laurentia and the western border of the Amazon Craton: Precambrian Research, v. 76, p. 213–227, doi: 10.1016/0301-9268(95)00026-7.

Santos, J. O. S., Rizzotto, G. J., Potter, P. E., McNaughton, N. J., Matos, R. S., Hartmann, L. A., Chemale, F., Jr., and Quadros, M. E. S., 2008, Age and autochthonous evolution of Sunsás Orogen in West Amazon Craton based on mapping and U-Pb geochronology: Precambrian Research, v. 165, p. 120–152, doi: 10.1016/j.precamres.2008.06.009.

Sato, K., Tassinari, C. C. G., Kawashita, K., and Petronilho, L., 1995, O Método Geocronológico Sm-Nd no IG/USP e suas aplicações: Anais da Academia Brasileira de Ciências, v. 67, p. 313–336.

Silva, E. L., ms, 1988, Geologia da região da Serra da Alegria, extremo sul do cráton Amazônico, município de Porto Murtinho—MS: São Paulo, Universidade de São Paulo, Instituto de Geociências, Dissertação (Mestrado), 147 p.

Steiger, R. H., and Jäger, E., 1977, Subcommision on Geochronology: Convention on the use of decay constants in geo- and cosmochronology: Earth Planetary Science Letters, v. 36, p. 359–362, doi: 10.1016/0012-821X(77)90060-7.

Tassinari, C. C. G., Medina, J., and Pinto, M. S., 1996a, Rb-Sr and Sm-Nd geochronology and isotope geochemistry of central Iberian metasedimentary rocks (Portugal): Geologie en Mijnbouw, v. 75, p. 69–79.

Tassinari, C. C. G., Cordani, U. G., Nutman, A. P., van Schmus, W. R., Bettencourt, J. S., and Taylor, P. N., 1996b, Geochronological systematics on basement rocks from the Rio Negro-Juruena Province (Amazonian Craton) and tectonic implications: International Geology Review, v. 38, p. 161–175, doi: 10.1080/00206819709465329.

Teixeira, W., Bettencourt, J. S., Girardi, V. A. V., Onoe, A. T., and Sato, K., 2006, Mesoproterozoic mantle heterogeneity in SW Amazonian Craton: $^{40}Ar/^{39}Ar$ and Nd-Sr evidence from mafic-felsic rocks, *in* Hansji, E., Mertanen, S., Rämö, T., and Vuollo, J., organizers, Dyke Swarms—time markers of crustal evolution: Proceedings of the Fifth International Dyke Conference: London, Taylor and Francis, v. 1, p. 113–129.

Teixeira, W., Geraldes, M. C., Matos-Salinas, G. R., Ruiz, A. S., Saes, G., and Vargas-Mattos, G., 2010, A review of the tectonic evolution of the Sunsás belt, SW portion of the Amazonian Craton: Journal of South American Earth Sciences, v. 29, p. 47–60, doi: 10.1016/j.jsames.2009.09.007.

Tollo, R. P., Corriveau, L., McLelland, J., and Bartholomew, M. J., 2004, Proterozoic tectonic evolution of the Grenville orogen in North America: An introduction: Geological Society of America Memoirs, v. 197, p. 1–8, doi: 10.1130/0-8137-1197-5.1.

Vasconcelos, P. M., Onoe, A. T., Kawashita, K., Soares, A. J., and Teixeira, W., 2002, $^{40}Ar/^{39}Ar$ geochronology at the Instituto de Geociências, USP: instrumentation, analytical procedures, and calibration: Anais da Academia Brasileira de Ciências, v. 74, n. 2, p. 297–342, doi: 10.1590/S0001-37652002000200008.

Wiens, F., ms, 1986, Zur lithostratigraphischen, petrographischen und strukturellen Entwicklung des Rio-Apa Hochlandes, Nordost Paraguay: Clausthal, Geologisches Institut der Technischen Universität Clausthal, Clausthaler Geowissenschaftliche, Ph. D. dissertation, 19, 280 p.

Williams, I. S., 1998, U-Th-Pb geochronology by ion microprobe, *in* McKibben, M. A., Shanks, W. C., and Ridley, W. I., editors, Applications of Microanalytical Techniques to Understanding Mineralizing Processes: Reviews in Economic Geology, v. 7, p. 1–35.

Zimmerman, U., 2005, Provenance studies of very low-to low-grade metasedimentary rocks of the Puncoviscana complex, northwest Argentina, *in* Vaughan, A. P. M., Leat, P. T., and Pankhurst, R. J., editors, Terrane Processes at the Margins of Gondwana: Geological Society, London, Special Publications, v. 246, p. 381–416, doi: 10.1144/GSL.SP.2005.246.01.16.